Can a halo CME from the limb be geoeffective?

Consuelo Cid, Hebe Cremades, Angels Aran, Cristina Mandrini, Blai Sanahuja, Brigitte Schmieder, Michel Menvielle, Luciano Rodriguez, Elena Saiz, Yolanda Cerrato, et al.

Can a halo CME from the limb be geoeffective?

C. Cid,[1] H. Cremades,[2] A. Aran,[3] C. Mandrini,[4,5] B. Sanahuja,[6] B. Schmieder,[7] M. Menvielle,[8,9] L. Rodriguez,[10] E. Saiz,[1] Y. Cerrato,[1] S. Dasso,[4,11] C. Jacobs,[12] C. Lathuillere,[13] and A. Zhukov[10]

Received 20 January 2012; revised 21 August 2012; accepted 16 September 2012; published 2 November 2012.

[1] The probability for a halo coronal mass ejection (CME) to be geoeffective is assumed to be higher the closer the CME launch site is located to the solar central meridian. However, events far from the central meridian may produce severe geomagnetic storms, like the case in April 2000. In this work, we study the possible geoeffectiveness of full halo CMEs with the source region situated at solar limb. For this task, we select all limb full halo (LFH) CMEs that occurred during solar cycle 23, and we search for signatures of geoeffectiveness between 1 and 5 days after the first appearance of each CME in the LASCO C2 field of view. When signatures of geomagnetic activity are observed in the selected time window, interplanetary data are carefully analyzed in order to look for the cause of the geomagnetic disturbance. Finally, a possible association between geoeffective interplanetary signatures and every LFH CME in solar cycle 23 is checked in order to decide on the CME's geoeffectiveness. After a detailed analysis of solar, interplanetary, and geomagnetic data, we conclude that of the 25 investigated events, there are only four geoeffective LFH CMEs, all coming from the west limb. The geoeffectiveness of these events seems to be moderate, turning to intense in two of them as a result of cumulative effects from previous mass ejections. We conclude that ejections from solar locations close to the west limb should be considered in space weather, at least as sources of moderate disturbances.

Citation: Cid, C., et al. (2012), Can a halo CME from the limb be geoeffective?, *J. Geophys. Res.*, *117*, A11102, doi:10.1029/2012JA017536.

1. Introduction

[2] Full halo coronal mass ejections (CMEs) are a particular class of CMEs that appears to surround the occulting disk of a coronagraph. The first report of a full halo CME (HCME) was provided by *Howard et al.* [1982] as consisting in a 2-D projection of solar material propagating approximately toward or away from the observer in the interplanetary (IP) space. Although nowadays it is well known that other propagation directions are consistent with the observation of these events, full halo CMEs erupting from the side of the Sun facing the Earth (front side) are considered to be a potential cause of major geomagnetic storms [e.g., *Gonzalez et al.*, 1994, 1999; *Schwenn*, 2006; *Zhang et al.*, 2007; *Bothmer and Zhukov*, 2007; *Gopalswamy et al.*, 2010c]. *Gopalswamy et al.* [2007] showed that the geoeffectiveness (as shown by the *Dst* index) of a halo CME declines with increasing distance of its source region from the central meridian. Although this paper uses a time window method that occasionally leads to an incorrect association between halo CMEs and geomagnetic storms, it provides a general understanding that disk center CMEs are more geoeffective and the geoeffectiveness declines when the source longitude moves away from the central meridian. *Zhao and Webb* [2003] showed that the association of front-sided full halo CMEs with moderate to large storms during the first half of solar cycle 23 tends to decrease as the solar cycle approaches its maximum, though this decreasing trend is not monotonic.

[1]Departamento de Física, Universidad de Alcalá, Alcalá de Henares, Spain.
[2]Universidad Tecnológica Nacional-Facultad Regional Mendoza/ CONICET, Mendoza, Argentina.
[3]Research and Scientific Support Department of European Space Agency, ESTEC, Noordwijk, Netherlands.
[4]Instituto de Astronomía y Física del Espacio, IAFE, CONICET-UBA, Buenos Aires, Argentina.
[5]Facultad de Ciencias Exactas y Naturales, UBA, Buenos Aires, Argentina.

Corresponding author: C. Cid, Departamento de Física, Universidad de Alcalá, Campus Universitario, Alcalá de Henares ES-28871, Spain. (consuelo.cid@uah.es)

0148-0227/12/2012JA017536

[6]Departament d'Astronomia i Meteorologia and Institut de Ciències del Cosmos, Universitat de Barcelona, Barcelona, Spain.
[7]Observatoire de Paris, LESIA, Meudon, France.
[8]CNRS/INSU, Université Versailles St-Quentin, LATMOS-IPSL, Guyancourt, France.
[9]Département des Sciences de la Terre, Université Paris-Sud, Orsay, France.
[10]Solar–Terrestrial Center of Excellence–SIDC, Royal Observatory of Belgium, Brussels, Belgium.
[11]Departamento de Física, Facultad de Ciencias Exactas y Naturales, UBA, Buenos Aires, Argentina.
[12]Centre for Plasma-Astrophysics, Department of Mathematics, K.U. Leuven, Leuven, Belgium.
[13]UJF-Grenoble 1/CNRS-INSU, Institut de Planétologie et d'Astrophysique de Grenoble, UMR 5274, Grenoble, France.

[3] *Gopalswamy et al.* [2010d] examined the IP counterparts of the 17 halo CMEs with source longitudes >45° (labeled as "limb halo CMEs" in that paper) and associated with intense (i.e., *Dst* < –100 nT) geomagnetic storms in the 1996–2005 period. These authors provide evidence that those geomagnetic storms are due to the sheath portion of the interplanetary CMEs (ICMEs). Moreover, they show that some of these storms are associated with interacting halo CMEs.

[4] *Zhang et al.* [2007] investigated the origin of all major geomagnetic storms (*Dst* < –100 nT) occurring during the time period 1996–2005. They conclude that about 60% of the events could be directly associated with a single CME and 27% of the events were caused by complex ejecta, originating from interacting CMEs. In particular, a case study [*Dasso et al.*, 2009] of the interaction between two ejecta around 0.5 AU has shown that the interaction of CMEs can produce serious consequences on predictions of CME geoeffectiveness, such as increasing the magnetic field (due to compression during the interaction) and modifying the time arrival (due to interchange of linear momentum between the interacting CMEs). High-speed solar wind streams emanating from coronal holes and creating corotating interaction regions were at the origin of the remaining 13% of severe geomagnetic storms in the study by *Zhang et al.* [2007]. In 68% of the cases, the associated CME appeared as a full halo CME. In 86% of the cases, the source of the geoeffective CMEs was located less than 45° from the central meridian position. Their investigation indicates that western events are more likely to be geoeffective than eastern events, in which case the sources of highly geoeffective events can extend to 85°W. This western bias was already shown by *Wang et al.* [2002]. From observations made by multiple spacecraft, it is known that CME shocks can be as wide as 180° [*Zurbuchen and Richardson*, 2006], and therefore a shock driven by a CME from the solar limb could reach the Earth. The question is how common those extremely wide CME-driven shocks are and, even more, whether or not they can be geoeffective when the Earth is hit by the extended sheaths behind them, if any.

[5] *Rodriguez et al.* [2009] studied three front-side halo CMEs with a nontypical geomagnetic response. Two of these events originated close to the central meridian. Contrary to what is expected from statistical studies [e.g., *Zhang et al.*, 2007], the halo CME on 4 April 2000, that originated far from the disk center is the one corresponding to the strongest geomagnetic disturbance among the three events studied. *Rodriguez et al.* [2009] noted that the CME's geomagnetic response (as measured, for example, by the *Dst* peak value) behaved correspondingly to the ICME signatures measured at L1 (more specifically, the north-south IP magnetic field component and the solar wind speed), meaning that the last step of the Sun-Earth chain (from L1 to the magnetosphere) is in accordance with what is expected. The event on 4 April 2000 was also discussed by *Gopalswamy* [2002]. This study, which compares the observations from the near-Sun region and in situ for the three largest geomagnetic storms of the year 2000, concentrates on issues related to the prediction of the 1 AU arrival of CMEs. As *Gopalswamy* [2002], *Rodriguez et al.* [2009] illustrated once again the need of checking the IP medium conditions to assure the existence of a physical relation between what departs from the Sun and what arrives to the Earth.

[6] Motivated by this idea, we performed a detailed analysis of the evolution, along the Sun-Earth chain, of the limb full halo (LFH) CMEs of solar cycle 23, by analyzing solar data (Hα, EUV corona, white light corona), IP type II emissions, solar energetic particle (SEP) data, solar wind data, and geomagnetic indices.

[7] This multidisciplinary study has been undertaken in the framework of an ISSI International Team project. This team, which joins scientists with expertise from the solar atmosphere to the terrestrial surface, was created because of the need to link all the steps of the Sun-Earth chain to perform accurate event studies. To our understanding, there are not so many deep-detailed multidisciplinary studies of such events, fully encompassing the from-Sun-to-Earth scenario. We should mention that *Gopalswamy et al.* [2010d] studied previously IP counterparts of what they called limb halo CMEs. However, the term limb halo CME was used for those halo CMEs with a source longitude >45°. In this paper, as will be described below, the term LFH CME refers to source longitude >80°. Moreover, *Gopalswamy et al.* [2010d] addressed only four events (of the 25 included in this paper) that have the source region longitude 80° or further from the central meridian (other events mentioned there are further from the limb).

[8] The paper is organized as follows. In section 2, we present the set of studied events and describe the analyzed data. In section 3, we review the solar source determination of every event and investigate the possibility of geomagnetic disturbance. In section 4, we revise IP data for those cases where we found geoeffectiveness in the analyzed temporal interval and revise the association between each LFH CME and the observed geomagnetic disturbance. Finally, in section 5, we present our conclusions.

2. Observations and Events

[9] The flow diagram in Figure 1 describes the procedure followed in our data analysis. The starting point for our study is the SOHO/Large Angle and Spectrometric Coronagraph (LASCO) halo CME catalog [*Gopalswamy et al.*, 2010a], available at http://cdaw.gsfc.nasa.gov/CME_list/halo/halo.html (a subset of the CME catalog by *Yashiro et al.* [2004] and *Gopalswamy et al.* [2009a]), from which we extract the list of LFH CMEs (only using events originating within 10° from the limb). Then, we revise the solar sources of each event of this list to verify that they are really halo events from the limb. The next step is to check the geoeffectiveness between 1 and 5 days after the LFH CME launch. The analysis of the events without geoeffective signatures stops at this point. Otherwise, we proceed with the study of the corresponding IP signatures. We check solar wind data from ACE/Solar Wind Electron, Proton, and Alpha Monitor (SWEPAM) and MAG [*McComas et al.*, 1998; *Smith et al.*, 1998], Wind/SWE [*Ogilvie et al.*, 1995], and Wind/Magnetic Fields Investigation [*Lepping et al.*, 1995]; SEP data from ACE/EPAM [*Gold et al.*, 1998] and GOES/EPS [*Sauer*, 1993]; and radio emission from Wind/WAVES [*Bougeret et al.*, 1995] data in order to support the possible association between the proposed LFH CME and the disturbance that caused the subsequent geoeffectiveness or not. In the latter case, we provide the inferred alternative geoeffective source (see Figure 1).

[10] It must be pointed out that type II (TII) radio emissions are used here to discard or reject possible associations between LFH CMEs and in situ disturbances. Given that the emission frequency and the density at the site of emission are directly

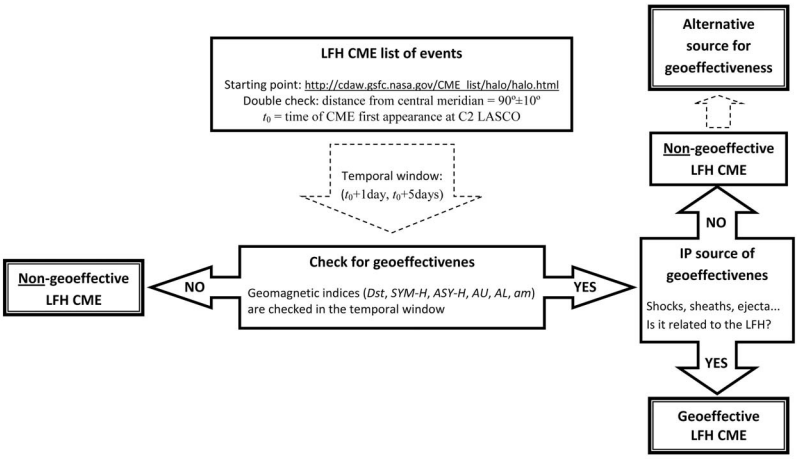

Figure 1. Flow diagram showing the methodology followed to analyze each LFH and its temporally related geoeffectiveness.

related, it is possible to determine the approximate distance from the Sun at which the emission takes place by using a density model (in this case, the one suggested by *Leblanc et al.* [1998]). TII emissions drifting down in frequency thus represent shocks entering into lower-density regions and moving away from the Sun. We are mostly interested in the kilometric frequency range (300–30 kHz), given that at those frequencies the shock is farther from the Sun and is considered to have undergone most of the deceleration, traveling at constant speeds and thus making it easier to relate it to a certain in situ disturbance. Although the Wind/WAVES type II listing at http://ssed.gsfc.nasa.gov/waves/ was consulted in a general basis for the existence of radio emissions, we have specifically checked the WAVES/TNR data, because of its improved resolution in most of the kilometric frequency range, of particular interest to us. Another consideration to bear in mind for interpretation of these data refers to the site of the emission, commonly assumed to be that of the shock's nose. The type II emission detected by the Wind/WAVES receivers could have originated at any portion of the vast CME shock extension, and there is a big chance that Wind/WAVES detects emissions arising from a parcel of shock traveling toward Earth than perpendicular or away from it, even if the speed of that parcel of shock is slower. The CME cases we analyze here are special, in that they all arise at the solar limbs and are all very energetic to be observed as halo CMEs nonetheless. For them, the drifting speed of the related type IIs is more likely to represent the speed of an Earth-directed portion of the shock (the flank) than the shock's nose. Therefore, here we use kilometric TIIs to infer shock arrival time at Earth, as a proxy to match LFH CME-related kilometric TII emissions with in situ signatures.

3. Event Analysis: Solar Origin and Terrestrial Response

3.1. Solar Source Determination

[11] As commented, we have selected all the LFH CMEs from the halo CME catalog. A description of the characteristics of halo CMEs can be found in *Howard et al.* [1982], *Gopalswamy et al.* [2004], *Gopalswamy et al.* [2003, 2007], and *Anonymous* [2005]. The term LFH CME refers in this paper to those full halo CMEs coming from the solar limb, i.e., W90 or E90. Therefore, we selected all full halo CMEs originating from either the western or the eastern limb during solar cycle 23 (from 1996 to 2009), according to the halo CME catalog. All events whose source region, as stated in the catalog, was within 10° of heliographic longitude from the solar east and west limbs (i.e., from −90° to −80° and from 80° to 90°, respectively) were also included, due to uncertainties in solar source determination close to the solar limbs. Events in the catalog associated with backside-limb sources ("Blimb" events) have not been taken into account here because of greater uncertainties in their real distance from the limb.

[12] For completeness, we have double-checked the heliographic coordinates of the selected events' source regions given in the catalog. We have independently identified the source location; characterized the corresponding active region and/or quiescent filament; and, in case the event was related to a flare, the flare characteristics, by using the following online and public databases.

[13] 1. X-ray flares and Hα flares reports from NOAA's Solar Geophysical Data Reports (ftp://ftp.ngdc.noaa.gov/STP/SOLAR_DATA/SGD_PDFversion/).

[14] 2. Active region (AR) NOAA numbers and locations (http://solarmonitor.org and http://www.solar.ifa.hawaii.edu/html/msoarmaps.shtml).

[15] 3. X-ray light curves from the Geostationary Environmental Satellites (http://www.solarmonitor.org/index.php).

[16] 4. Daily magnetograms from the Michelson Doppler Imager onboard SOHO spacecraft (SOHO/MDI) (http://soi.stanford.edu/production/mag_gifs.html).

[17] 5. Daily movies from the Extreme-Ultraviolet Imaging Telescope (SOHO/EIT [*Delaboudinière et al.*, 1995]) in 195 Å from the Institut d'Astrophysique Spatiale, MEDOC data center (http://www.ias.u-psud.fr/eit/movies/) and from the LASCO CME catalog (http://cdaw.gsfc.nasa.gov/CME_list/).

[18] 6. Hα observations from the Paris Observatory, Meudon (http://bass2000.obspm.fr) and from the Big Bear

Solar Observatory and the Hα network (http://www.bbso.njit.edu/Research/FDHA/).

[19] Table 1 lists the final set of 25 LFH CMEs considered in this study. The first part of Table 1 gives information about the solar source and characteristics of each event, whereas the second part indicates the observed geomagnetic activity (to be described in the next section). The first column of Table 1 gives the number assigned to each event. Columns 2–9 give information about the solar event (source-related activity and LFH CME): date (day/month/year; day of year (DoY)), time of first appearance in the field of view of the LASCO/C2 coronagraph, plane-of-the-sky speed from linear fitting (from http://cdaw.gsfc.nasa.gov/CME_list/), 1–8 Å X-ray flare class registered by GOES satellites, time of flare maximum intensity, type of solar source (i.e., NOAA AR number and/or filament eruption when quiescent filament eruption was observed or inferred), and source location of either the associated solar flare or the filament eruption in the case of no reported associated flare. The source of the CME is expressed in heliographic coordinates and corresponds to the position of the associated flare at the onset time or to the position of the filament eruption on the disk at the time of the CME. Note that according to the halo CME catalog, the "source location" property of the selected CMEs is within 10° from the solar east and west limbs (i.e., from −90° to −80° and from 80° to 90° heliographic longitude, respectively). It is worth pointing out that the AR or quiescent filament central coordinates shown in Table 1 might differ from those of the catalog, since the latter corresponds to the GOES flare site in the case of ARs and central location in the case of filament eruptions. Furthermore, this difference in source location coordinates between Table 1 and the halo CME catalog is, at most by a few degrees, what can be considered small when compared to the extension of flares belonging to large events and within a reasonable uncertainty in location determination close to the limbs. When the source is an AR and it had not appeared on the Sun's visible side by the time of the ejection, as may happen for CME events launched close to the east solar limb, the AR number assigned is deduced by taking into account the mean solar rotation rate at the corresponding latitude (these cases are marked in Table 1 with the superscript b). If an AR is observed at that latitude later on and a number was allotted to it, the CME is associated with this AR. When the brightening occurs at the limb and the precise heliographic longitude of the possible associated flare is not known, the longitude of the flare is indicated as E90 or W90.

[20] Two CMEs initially included in the subset list of LFH CMEs were finally discarded: the CME on 26 June 2005 at 07:54 UT (reported to arise from N15E80) and the CME on 4 January 2002 at 09:30:05 UT (reported from N38E87). When looking at the EIT movie for the 26 June 2005 CME, we identified a B5.0 flare located at N15, probably coming from a region just behind the limb. The flare is situated quite close to the equator (Figure 2 (left), arrow). However, the observed CME (Figures 2 (middle) and 2 (right)), which is ejected along a different direction (NNE), has its source clearly >10° away from the limb (as indicated by its projected morphology), and therefore it is most likely not associated with the B5.0 flare. The reason for having discarded the second event, the CME on 4 January 2002, is the difficulty to unambiguously determine its source region location. The eruption of a filament at N25E70 is clearly associated with the CME. However, those coordinates correspond to the center of the visible part of a filament that could continue to the back side. A posteruptive flare is reported close to the east limb although no coordinates are reported by GOES. Therefore, due to the inability to determine the coordinates of the filament eruption, it is not included in the list.

[21] Most of the studied LFH CMEs in Table 1 are associated with flares located in ARs, in agreement with previous results [*Gopalswamy*, 2010] . The eruptions and flares are well identified in 195 Å EIT movies by the opening of coronal loops, enhancement of EUV emission, and/or the development of postflare loops. In several cases, post-flare loops were also observed as bright arcades at the limb in Hα.

[22] For one event (29 July 2004) no limb active region could be identified as the source of the LFH CME. Nevertheless, in this case the eruption of a filament was observed around the onset time of the CME together with the formation of interconnecting loops between two active regions (Figure 3). Therefore, we propose the filament as the most plausible source of the CME. From a statistical point of view, around 15% of CMEs originate from filament eruptions not related to active regions [*Dere and Subramanian*, 2001].

3.2. Terrestrial Environment Analysis

[23] The second step in the procedure corresponds to the analysis of data related to geomagnetic disturbances. The interval of geoeffectiveness explored extends between 1 and 5 days after the LFH CME appearance at LASCO/C2; we check this time interval for all the events in Table 1. We treated this as a Yes/No answer to the question "Is there any kind of geoeffectiveness in that temporal window?", despite that such an answer is not always straightforward. The *Dst* index is commonly used to determine if an event is geoeffective or not: an event is classified as geoeffective if its *Dst* index decreases below −50 nT [*Gonzalez et al.*, 1994]. Nevertheless, sometimes solar activity disturbs the terrestrial environment while the *Dst* index remains quiet. For that reason, we have also checked the *SYM-H* and the *ASY-H* indices, as proxies for the low-latitude disturbances; the *AU* and *AL* indices, as proxies for high-latitude disturbances; and, finally, the *am* index, as a proxy for planetary disturbance. A short description of these indices is given below (we refer to *Menvielle and Berthelier* [1991] and *Menvielle et al.* [2011] for an extensive description of the geomagnetic indices); reference values of these geomagnetic indices can be found at the WDC-C2 for Geomagnetism, Kyoto, Japan (http://swdcwww.kugi.kyoto-u.ac.jp/), and International Service of Geomagnetic Indices (hosted by LATMOS, Guyancourt, France; http://isgi.latmos.ipsl.fr/).

[24] 1. The *Dst* index, derived on a 1 h basis, measures the variations in the geomagnetic horizontal component at four low-latitude observatories [*Sugiura*, 1964; *Sugiura and Kamei*, 1991]. It monitors the axis-symmetric part of the magnetospheric currents, including mainly the ring current, but also the magnetopause Chapman-Ferraro current. The *SYM-H* index [*Iyemori et al.*, 1992] is essentially the same as the *Dst* index, but with the advantage of being derived on a 1 min basis and from a set of six stations, or groups of stations. It is worth noting that both *Dst* and *SYM-H* zero values have no physical meaning.

Table 1. Solar and Geomagnetic Activity[a]

		Solar Activity							Geomagnetic Activity							
									Dst							
Event Number	CME Date	DoY	CME Time (UT)	CME Speed (km/s)	Flare Class	Flare Maximum (UT)	Solar Source Type	Flare Location	Dst_{min} (nT)	Dst_{min} Date (DoY/hh)	*SYM-H*	*ASY-H*	*AL*	*AU*	*am*	G?	Geoeffective Source
1	23/4/1998	113	05:55:22	1691	X1.2	05:55	AR8210[b]	S18E90	−69	114/08	Y	Y	Y	Y	Y	G	Filament eruption
2	24/11/1998	328	02:30:05	1798	X1.0	02:20	AR8384[b]	S25W90	−23	329/22	N	N	N	N	N	-	
3	25/7/1999	206	13:31:21	1389	M2.4	13:38	AR8639	N38W81	−38	210/03	N	N	*	Y	N	-	
4	5/5/2000	126	15:50:05	1594	M1.5	16:21	AR8976 &AR8977[b]	S14W90	−23	131/02	N	*	*	N	N	-	
5	16/10/2000	290	07:27:21	1336	M2.5	07:28	AR09182[b]	N03W90	−19	293/00	N	N	N	N	N	-	
6	1/4/2001	091	11:26:06	1475	M5.5	12:17	AR09415[b]	S22E90	−387[c]	090/09	N	*	*	*	N	-	
7	1/10/2001	274	05:30:05	1405	M9.1	05:15	AR9628	S18W90	−166	276/15	Y	Y	Y	Y	Y	G	AR9636 & LFH
8	14/12/2001	348	09:06:06	1506	M3.5	09:13	AR9742	N09E90	−39	351/22	N	*	*	N	N	-	
9	28/12/2001	362	20:30:05	2216	X3.4	20:45	AR9767[b]	S23E90	−58	364/06	Y	Y	Y	*	*	G	AR9742
10	10/3/2002	069	23:06:05	1429	M2.3	23:25	AR9871[b]	S21E90	−11	071/10	N	N	N	N	N	-	
11	22/3/2002	081	11:06:05	1750	M1.6	11:14	AR9866 &AR9870[b]	S09W90	−100	083/10	Y	Y	Y	Y	Y	G	AR9866 & AR9870
12	21/4/2002	111	01:27:20	2393	X1.5	01:51	AR9906	S14W84	−57	113/16	Y	Y	Y	Y	Y	G	LFH CME
13	19/7/2002	200	16:30:05	2047	No flare	–	Unnumbered region[b]	S21E90	−38	203/10	N	N	*	*	N	-	
14	20/7/2002	201	22:06:09	1941	X3.3	21:30	AR10039	S13E90	−38	203/10	N	N	N	N	N	-	
15	24/8/2002	236	01:27:19	1913	X3.1	01:12	AR10069	S02W81	−45	238/20	N	*	*	Y	*	-	
16	15/6/2003	166	23:54:05	2053	X1.3	23:56	AR10386	S07E80	−141	169/10	Y	Y	Y	Y	Y	G	LFH CME
17	4/11/2003	308	19:54:05	2657	X28	19:50	AR10486	S19W83	−33	313/20	N	Y	Y	*	Y	G	LFH CME
18	29/7/2004	211	12:06:05	1180	C2.1	13:04	Filament eruption & AR10652 & AR10653	S07W88	−40	214/02	N	N	N	N	N	-	
19	3/6/2005	154	12:32:10	1679	M1.0	12:26	AR10775[b]	N15E90	−43	158/06	N	N	N	N	N	-	
20	13/7/2005	194	14:30:05	1423	M5.0	14:49	AR10786	N11W90	−67	199/07	N	N	*	N	N	-	
21	14/7/2005	195	10:54:05	2115	X1.2	10:55	AR10786	N11W90	−67	199/07	Y	Y	Y	Y	Y	G	AR10786
22	27/7/2005	208	04:54:05	1787	M3.7	05:02	AR10792[b]	N11E90	−41	209/06	Y	Y	Y	Y	Y	G	CH & backside halo
23	23/8/2005	235	14:54:05	1929	M2.7	14:44	AR10798	S14W90	−184[c]	236/12	Y	Y	Y	Y	Y	-	
24	5/9/2005	248	09:48:05	2326	C2.7	10:41	AR10808[b]	S07E81	−36	252/23	N	N	N	N	N	-	
25	25/1/2007	025	06:54:04	1367	C6.3	07:14	AR10940	S08E90	−49	029/22	Y	Y	Y	Y	Y	G	CH

[a]The first column indicates the event number in our list. The second to ninth columns show solar data related to the LFH CME: date (day/month/year, column 2), day of year (DoY, column 3), time of first appearance in the LASCO C2 coronagraph (column 4), plane-of-the-sky speed from linear fitting (as reported in http://cdaw.gsfc.nasa.gov/CME_list/, column 5), X-class flare (column 6), time of flare maximum as registered by GOES satellite in soft X-rays (column 7), type of solar source (i.e., AR identified by its NOAA number and/or filament eruption when the eruption of a quiescent filament was observed) (column 8), and associated solar flare or filament eruption location (when no associated flare is reported) (column 9). The results for different indices analyzed are shown in columns 10–16. Column 10 shows the minimum value of the *Dst* index in the interval from 1 day after the CME onset until 5 days later. The date (DoY/hour) of reaching this minimum value appears in column 11 (see text for details). The Dst_{peak} value of the storm is provided, instead of the Dst_{min} value in the interval analyzed. In this case, the date in column 11 corresponds to the date of the Dst_{peak}. The 12th to 16th columns show the geoeffectiveness as seen by the indices *SYM-H* (column 12), *ASY-H* (column 13), *AU* (column 14), *AL* (column 15), and *am* (column 16) as Y (geoeffective), N (nongeoeffective), or * (the index is disturbed, but not enough to be classified as geoeffective). As a summary of the activity at the terrestrial environment, column 17 indicates if the interval analyzed is geoeffective (G) or not (−). Column 18 includes the source of the geoeffectiveness for those events where a G has been fixed in the previous column.

[b]Active regions were located in the backside of the Sun close to the limb at first appearance in LASCO C2.

[c]The time window analyzed in the *Dst* index is recovering from a previous storm.

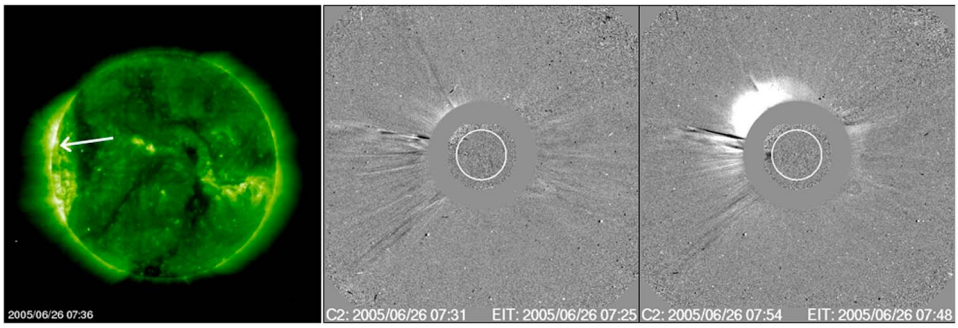

Figure 2. (left) EIT image in 195 Å showing the location of the B05 flare on 26 June 2005 at 07:36 UT. The arrow points to a set of newly faint formed loops that can be seen growing at the eastern limb. (middle and right) Two LASCO C2 images at the time of appearance of the CME in the NNE limb (Figure 2, middle) and as it evolved at 07:54 UT (Figure 2, right).

[25] 2. The *ASY-H* index [*Iyemori et al.*, 1992], derived on a 1 min basis from the same network of stations as *SYM-H*, monitors both the direct and the unloading response of the magnetosphere (partial ring current).

[26] 3. The *AU* and *AL* indices [*Davis and Sugiura*, 1966], currently derived on a 1 min basis, are based on the variations in the geomagnetic north-south component at 11 observatories distributed in longitude over the auroral oval. They are intended to represent a measure of the maximum current density of the eastward and westward auroral electrojets, respectively. They monitor the magnetic activity produced by enhanced ionosphere currents in the auroral zone, mostly related to the magnetosphere-ionosphere coupling through the field-aligned currents.

[27] 4. The *am* planetary geomagnetic index [*Mayaud*, 1968] is a weighted average of the *aK* equivalent amplitudes derived from 3 h range *K* indices measured at a network of currently 22 subauroral latitude stations evenly distributed in longitude in both hemispheres. It is statistically related to the overall magnetosphere energy status.

[28] Up to now, threshold values for classifying the geoeffectiveness of an event have been only established for the *Dst* index [e.g., *Gonzalez et al.*, 1994; *Zhang et al.*, 2006]. Therefore, for other geomagnetic indices, visual inspection of data is the only way to identify the presence of a disturbance. Columns 10–16 of Table 1 show the results for the indices analyzed: columns 10 and 11, respectively, show the minimum value of the *Dst* index attained within the inspected time interval and the time (DoY/hour) of occurrence of this minimum value. In quiet time periods, with the *Dst* index slightly fluctuating, column 11 only indicates the first time when the minimum value was registered.

[29] For two events (Table 1, #6 and #23), the *Dst* index was recovering from previous intense storms, and the minimum value for the *Dst* appears at the beginning of the data interval analyzed. Although this value is below −50 nT, it does not mean that the event can be considered geoeffective, as it corresponds to a previous event. Therefore, if there is not any other significant decrease in the interval analyzed where the threshold of −50 nT is passed again, we indicate that the *Dst* peak corresponds to the previous storm (these cases are marked in Table 1 with the superscript c) and the LFH event is considered nongeoeffective.

[30] Successive columns from 12 to 16 in Table 1 show whether there is geoeffectiveness (indicated as Y) or not (indicated as N) in the temporal interval established, respectively, according to the *SYM-H*, *ASY-H*, *AU*, *AL*, and *am* indices. An asterisk indicates the existence of a noticeable disturbance, but not intense enough to be classified as geoeffective according to the corresponding index.

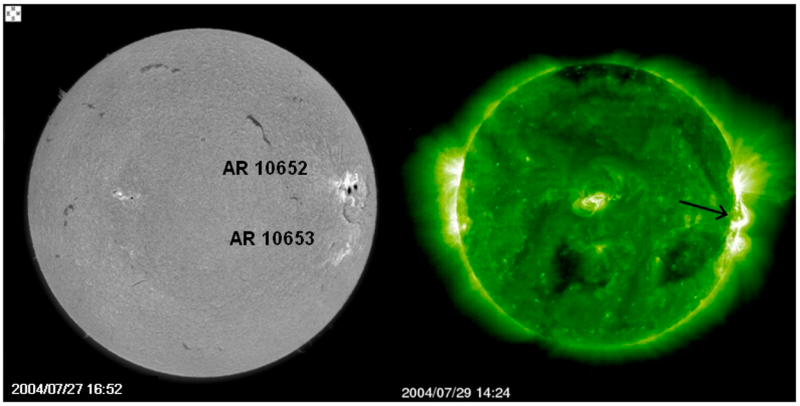

Figure 3. (left) Hα image obtained at Big Bear Solar Observatory showing the two ARs and the filament between them 2 days before its eruption. (right) EIT image in 195 Å after flare maximum showing the formation of interconnecting loops between AR 10652 and 10653 (pointed by an arrow).

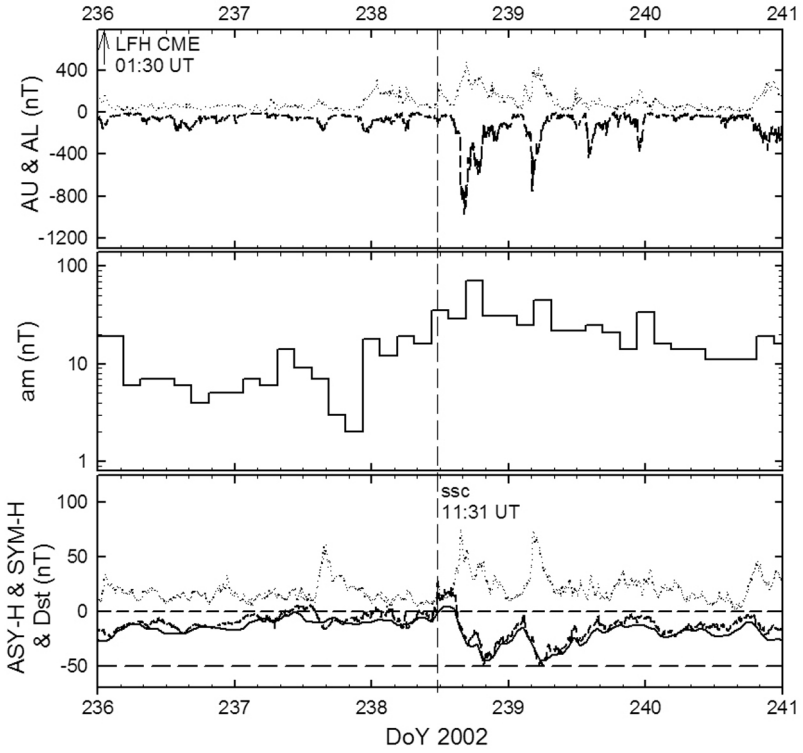

Figure 4. Geomagnetic indices for the time period 24–28 August 2002. (top) The *AU* (dotted line) and *AL* (short dashed line) indices. (middle) The *am* planetary geomagnetic index. (bottom) The *Dst* (solid line), *SYM-H* (short dashed line), and *ASY-H* (dotted line) indices. Horizontal dashed lines Figure 4 (bottom) indicate zero value and −50 nT (threshold value for geoeffectiveness according to the *Dst* index). The vertical line marks the time of an *ssc* (see text for details). An arrow in Figure 4 (top) indicates the time of first appearance in the field of view of the LASCO/C2 coronagraph of the LFH CME on 24 August 2002.

[31] In the following, we consider that an event is geoeffective (labeled as G in column 17) either if the *Dst* index reaches a minimum value below −50 nT, or if a disturbance above background level appears simultaneously in all indices analyzed (even though the minimum value of *Dst* is above −50 nT). Several events are described below to illustrate the information displayed in Table 1.

[32] Figure 4 presents geomagnetic indices for the time period 24–28 August 2002. A LFH CME occurred on 24 August 2002 (DoY 236) at 01:27:19 UT (event #15), and a storm sudden commencement (*ssc*) occurred on 26 August (DoY 238) at 11:31 UT (Figure 4, vertical line). This *ssc* is most likely associated with the sharp compression of the magnetosphere corresponding to the arrival of an IP shock at Earth's orbit. During the following 24 h, the *Dst* reaches twice minimum values of about −45 nT. In the meantime, significant variations can be observed on the other indices in a context of geomagnetic activity that started more than 1 day before the *ssc*. The *ssc* marks the beginning of a more active period for *AU*, while this is not so clearly the case for *AL*, *am*, and *ASY-H*. Therefore, in this event, geoeffectiveness for the *AU* index has been indicated as Y in Table 1, while an asterisk appears for the other indices. The *SYM-H* index is flagged with an N, considering the same threshold as for the *Dst*. Since the *ssc* and the associated magnetic event only correspond to a clear increase of geomagnetic activity at high latitudes, we considered this event as nongeoeffective.

[33] Figure 5 presents the aforementioned geomagnetic indices for event #17 (4–8 November 2003). An *ssc* occurred on 4 November at 6:25:00 UT (Figure 5, solid vertical line); this is before the LFH CME onset (4 November, DoY 308, at 19:54:05 UT); consequently, it cannot be associated with this solar event. One day after the LFH CME onset, at the beginning of the period to analyze the terrestrial environment, the *Dst* index is still recovering from this previous event, which reached values below −50 nT. On 6 November (DoY 310), about 2 days after the CME onset, a sharp increase in *SYM-H* is observed at around 19:40 UT (Figure 5, dashed line). This time marks the beginning of a few hours-long very active period that is observed on all indices, and thus at all latitudes. In addition, this active period is preceded and followed at all latitudes by periods of low magnetic activity. We therefore consider this event as geoeffective although the *Dst* and *SYM-H* indices did not fall below the −50 nT threshold.

[34] From this analysis, we conclude that 15 of the 25 studied LFH CME events (Table 1) are not geoeffective. Following the procedure described in the flowchart of Table 1, their analysis ends here. For the other 10 (Table 1, events marked G in column 17), the last column of Table 1 indicates the solar source that we deduced from our detailed analysis as

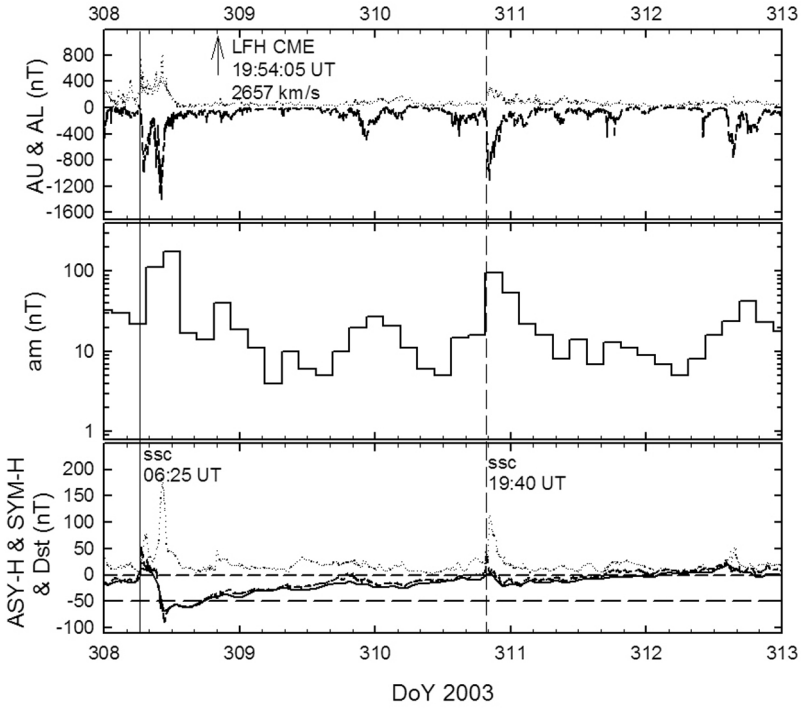

Figure 5. Geomagnetic indices for the time period 4–8 November 2003. The format is the same as that of Figure 4. The solid and dashed vertical lines mark the time of two storm sudden commencements (see text for details). An arrow in the top panel indicates the time of first appearance in the field of view of the LASCO/C2 coronagraph of the LFH CME on 4 November 2003.

the origin of the observed geoeffectivity, as discussed in next section. When this source does not correspond with the studied LFH CME, we indicate in this last column the launch location of the proposed source; otherwise, we mention that the considered LFH CME is geoeffective. In this latter case, the geoeffectiveness can be attributed to the CME itself, or to the CME in combination with other CMEs. These events are discussed in detail in section 4.

4. Event Analysis: Interplanetary Space

[35] The following step in the procedure is the analysis of the interplanetary space data (see Figure 1), by looking at data of the solar wind, energetic particles, and radio emission. Interplanetary magnetic field (IMF) and solar wind plasma data from Wind and ACE spacecraft were inspected for the 10 geoeffective events identified. The objective is to look for the IP causes of the geoeffectiveness observed within the 5 day time window after the LFH CME launch date. Those events where the terrestrial environment disturbance is not related to the LFH CME are described in section 4.1. The events for which a complete observational Sun-to-Earth chain can be established, and where the LFH CME can be identified as the trigger of the terrestrial disturbance, are analyzed in full detail in section 4.2.

4.1. LFH CMEs Not Associated With the Prescribed Geomagnetic Disturbance

4.1.1. Event #1 (23 April 1998)

[36] On 23 April 1998 (DoY 113) at 17:28 UT, the ACE spacecraft detected the passage of an IP forward shock that preceded the *ssc* observed in the *Dst* index behavior, followed by a drop down to −69 nT (see Figure 6). This shock (Figure 6, solid line) was the only one detected within ∼16 days prior to the *Dst* minimum. The LFH CME associated with this *Dst* minimum by *Gopalswamy et al.* [2007] was first detected by the LASCO/C2 coronagraph at 05:55 UT on 23 April. However, the solar wind speed observed by ACE remained below 500 km s^{-1} for more than 3 days before the shock arrival, making it unlikely that a shock driven by this CME arrived to ACE in less than 12 h. Hence, this LFH CME is not the trigger of the observed geomagnetic disturbance.

[37] On 26 April (DoY 116) at 17:00 UT, a second peak (minimum) appears in the *Dst* index. This peak is related to a discontinuity observed in the B_y component of the IMF in geocentric solar magnetospheric (GSM) coordinates, together with a drop in the solar wind density (Figure 6, dashed line), characteristic of reverse shocks. However, no other signature in the solar wind velocity or in the magnetic field allows the identification of this density disturbance as a shock. Moreover, no other ICME signature appears in the IP plasma and magnetic field data. Consequently, there is no evidence in the 1 AU in situ data that relates the drop on the *Dst* index time profile on 26 April to the LFH CME on 23 April. Hence, this CME from the limb was not geoeffective.

[38] The energetic particle intensity-time profiles measured prior to the *Dst* peak on 24 April (DoY 114) and type II kilometric radio emission help to associate the IP shock on 23 April with a partial halo (PH) CME from the west limb. *Nitta et al.* [2003] reported that the solar origin of the measured large SEP event is the PH CME first seen by the

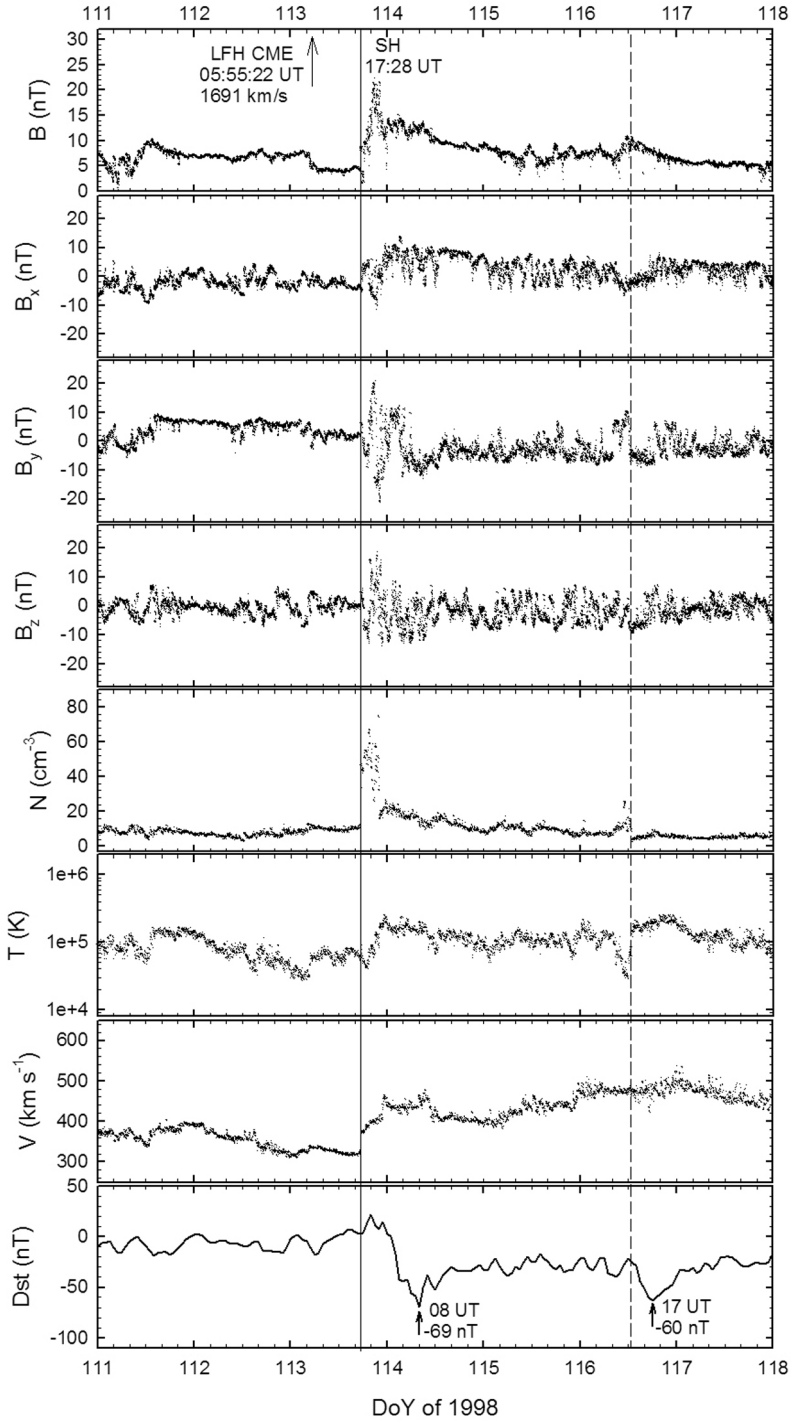

Figure 6. Interplanetary data and *Dst* index for event #1. An arrow in the first panel indicates the time of first appearance in the field of view of the LASCO/C2 coronagraph of the LFH CME on 23 April 1998. Shown, from top to bottom, are the magnetic field intensity and the magnetic field components in GSM coordinates (measured by ACE/MAG) and the solar wind density, temperature, and speed (measured by ACE/SWEPAM). The solid (dashed) vertical line indicates the passage of a forward (reverse) IP shock by ACE. The eighth panel shows the *Dst* index.

LASCO C2 coronagraph at 10:07 UT on 20 April. This PH CME is in temporal association with an M1.4 flare, located at S30W90, that peaked at 10:21 UT on the same day. *Gopalswamy et al.* [2004, 2005a] used also type II metric and decameter hectometric radio emission to establish the association between the SEP event with this same flare and CME. Therefore, the IP shock on 23 April was associated with this PH CME [e.g., *Tylka et al.*, 2000; *Reames et al.*,

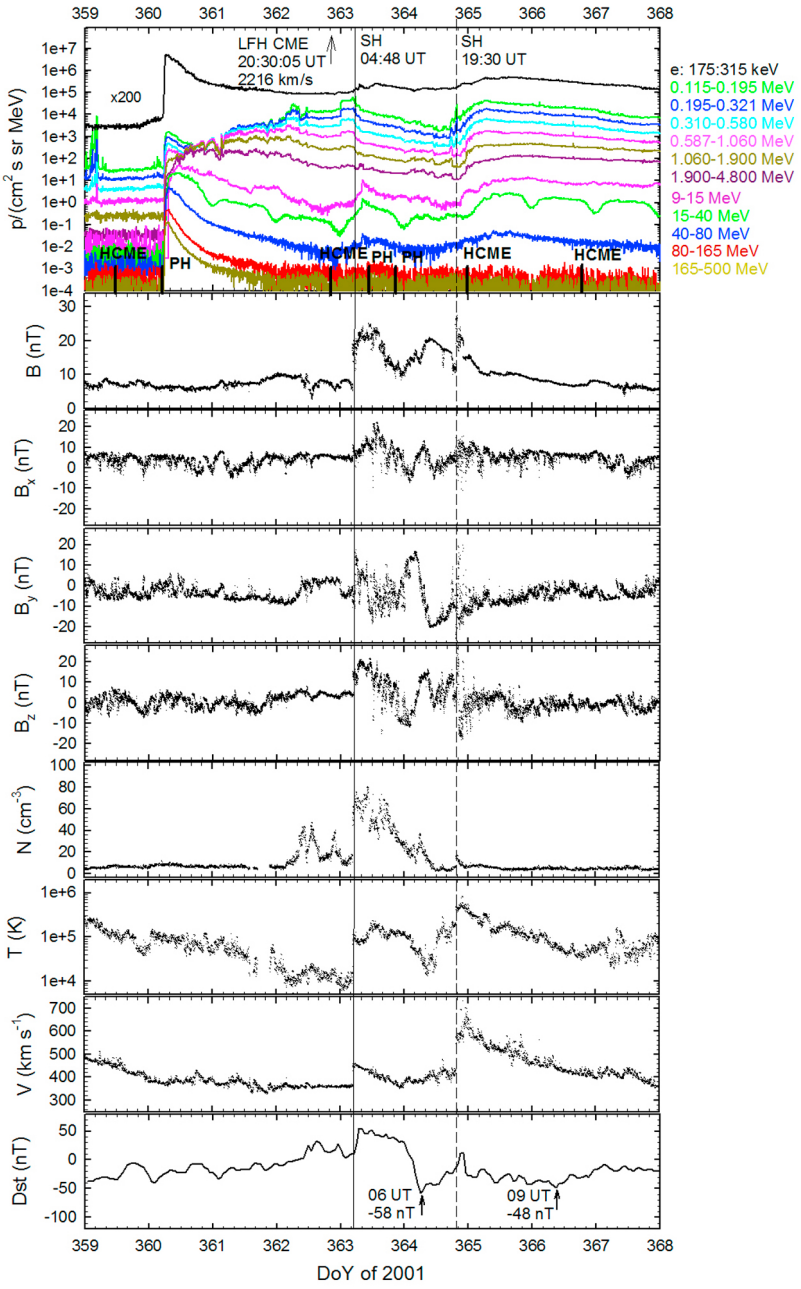

Figure 7. Interplanetary data and *Dst* index for event #9. An arrow in the first panel indicates the time of first appearance in the field of view of the LASCO/C2 coronagraph of the LFH CME on 28 December 2001. The first panel shows proton intensity-time profiles measured by the ACE/EPAM/LEMS120 detector, from 0.115 to 4.8 MeV (color coded) and by the GOES-8/SEM/EPS detector, from 9 to 500 MeV. The black trace corresponds to the 115–315 keV electron intensity measured by the ACE/EPAM/DE30 detector, multiplied by 200 as indicated. Short vertical lines mark the time of the first appearance by the SOHO/LASCO/C2 coronagraph of halo and partial halo CMEs (labeled HCME and PH, respectively). Shown, from top to bottom, are the magnetic field intensity and the magnetic field components in GSM coordinates (measured by ACE/MAG) and the solar wind density, temperature and speed (measured by ACE/SWEPAM). The two vertical lines indicate the passage of forward IP shocks by ACE. The ninth panel shows the *Dst* index. Arrows in the ninth panel mark the time of minimum values of the *Dst* index.

2001; *Gopalswamy et al.*, 2001, 2010b]. Since there is no other IP signature of a transient event, the geomagnetic activity observed in the analyzed temporal window may be attributed to the PH CME on 20 April 1998.

4.1.2. Event #9 (28 December 2001)

[39] Figure 7 illustrates the SEPs' enhancements, solar wind, and IMF conditions measured during the events of the last 6 days of December 2001 and the beginning of January

2002, from 25 December (DoY 359) to 2 January 2002 (DoY 367). The seven short vertical lines in Figure 7 (first panel) mark the time of first appearance of the observed HCMEs and PH CMEs in the SOHO/LASCO/C2 coronagraph. The two vertical lines mark the time of the passage of the two IP shocks detected by ACE in the time period displayed: the first on 29 December (DoY 363) at 04:48 UT, with a background solar wind speed of ~450 km s^{-1}, and the second on 30 December at 19:30 UT, with a solar wind speed of ~600 km s^{-1}, previously reported, among others, by *Gopalswamy et al.*, [2010b]. No signatures of magnetic cloud driving any shock can be identified. Two *ssc* are clearly seen in the *Dst* index (Figure 7, ninth panel) due to the compression of the magnetosphere corresponding to the arrival of both IP shocks at the Earth orbit; these *ssc* indicate two different geomagnetic events, although the second one takes place during the recovery phase of the first one. The two arrows in Figure 7 (ninth panel) indicate the time when *Dst* minima occurred, on 30 December 2001 at 06:00 UT (−58 nT) and on 1 January 2002 at 09:00 UT (−48 nT). The HCME marked also with an arrow in Figure 7 (first panel) is the LFH CME on 28 December 2001 (DoY 362); it appeared in LASCO/C2 at 20:30 UT, originating from AR9767 located at a latitude of ~23° south and just behind the east limb. This LFH CME was the source of the *Dst* peak on 30 December (Figure 7, first arrow) according to *Gopalswamy et al.* [2007].

[40] As can be seen in Figure 7 (first panel), a gradual SEP event started on 26 December (DoY 360). High-energy (>40 MeV) protons and near-relativistic electron intensities rapidly increase after the occurrence of a PH CME on 26 December at 05:30 UT, arising from AR9742 at N08W54. This PH CME was associated with a M7.1/1B flare starting at 04:32 UT that same day [e.g., *Gopalswamy et al.*, 2004; *Agueda et al.*, 2009]. *Gopalswamy et al.* [2005a] associated the PH CME and type II radio emission with the onset of the SEP event. The prompt rise seen at the low energy (<5 MeV) proton intensities is due to electron contamination [*Lario et al.*, 2004, and references therein]. This SEP event exhibits the characteristic profiles of a well-connected event, as its solar source confirms. The high-energy intensities rapidly increase at the beginning of the event, when the IP shock driven by the PH CME is still close to the Sun and strong (note that the observer is magnetically connected to the nose of the shock at that time). Later on, its efficiency at accelerating high-energy particles rapidly decreases. This lack of efficiency is smoothly translated to lower energies as the shock moves away from the Sun, and the observer's connection slides toward the eastern flank of the shock front. In this way, particle intensities start decreasing before the shock arrival at ACE, and only the flux profiles of $E < 0.5$ MeV protons keep increasing and peak at the shock passage on 29 December (Figure 7, solid line). The association of this IP shock with the PH CME on 26 December is confirmed by the type II radio emission profile. We argue that this IP shock and its driver, the PH CME, triggered the geomagnetic activity that yield the *Dst* peak on 30 December (Figure 7, first arrow). *Cane and Richardson* [2003] and *Cane et al.* [2006] related a disturbance (*ssc*) on 29 December at 05:38 UT and the passage of an ICME (30 December, 00:00–14:00 UT) with the PH CME on 26 December. This association agrees with our interpretation. Moreover, both the time elapsed from the onset of the LFH CME and the IP shock on 29 December, only 7 h 18 min, and the measured solar wind speed after the shock passage render impossible that this LFH CME were the cause of the geoeffective disturbance on early 30 December.

[41] The type II radio emission after the LFH CME on 28 December present in Wind/WAVES RAD1 (also in accordance with *Gopalswamy et al.* [2005a], as occurs with other events analyzed here) indicates the presence of an IP shock traveling at ~830 km s^{-1}, with an expected arrival time at ~00:00 UT on 31 December. The shock speed was derived from the profile of a type II emission seen to drift from ~1000 to 400 kHz in the RAD1 dynamic spectrum, which corresponds to radial distances in the range ~11–25 solar radii (R_s) from the Sun when assuming a local plasma frequency at Wind equal to 7.2 cm^{-3}. Disparities between the TII-derived speed and the LASCO plane-of-sky propagation speed are likely due to different speeds held by the shock's flank (propagating fairly toward Earth) and the CME's leading edge (propagating perpendicular to the Sun-Earth line), as addressed in section 2. For this event, we have made an exception by considering hectometric wavelengths, to have another means of discarding the association between the LFH CME on 28 December and the geoeffectiveness starting on 30 December. *Cane et al.* [2006] associated the LFH CME with the IP shock on 30 December at 19:30 (Figure 7, dashed line). Even if this LFH CME contributed to the geomagnetic disturbance recorded on 1 January 2002 together with the following PH CMEs, the *Dst* index remained above −50 nT, and the rest of the geomagnetic indices did not indicate any remarkable disturbance over the background; thus, the LFH on 28 December 2001 was not geoeffective.

4.1.3. Event #11 (22 March 2002)

[42] On 22 March 2002 (DoY 81) at 11:06 UT, a LFH CME appeared in the LASCO/C2's field of view. It arose from the interaction between AR9866 and AR9870, centered ~15° south on the west limb. Geoeffectiveness began about 1 day after this LFH CME (Figure 8), and the *Dst* minimum (−100 nT) is reached at 10:00 UT on 24 March (DoY 83). This geomagnetic disturbance, which started on 23 March at about 11:00 UT, was related to a big ICME (and preceding the postshock compression region) detected by ACE starting on 24 March at 12:00 UT and lasting until 25 March at 20:00 UT (http://www.ssg.sr.unh.edu/mag/ace/ACElists/ICMEtable.html). Although there is a clear depression in temperature during the ICME passage (Figure 8, shadowed area), temperature increases at the beginning of 25 March at the same time that density, velocity, and magnetic field strength show a clear discontinuity at 00:57 UT (Figure 8, dashed line), indicating that the big ICME might be a MultiMC [*Wang et al.*, 2003] or a complex ejecta [*Burlaga et al.*, 2002]. This ICME was driving an IP shock that arrived at ACE on 23 March at 10:53 UT (Figure 8, solid line), only ~24 h after the aforementioned CME on 22 March. This, together with the fact that the solar wind speed downstream of the IP shock reached only ~482 km s^{-1}, makes the association of this IP shock with this LFH CME unlikely according to data gathered at 1 AU. Hence, this LFH CME did not trigger the geoeffectiveness of the disturbance on 24 March. On 25 March (DoY 84) at 00:57 UT, there is a shock-like discontinuity in the magnetic field strength and solar wind speed. It might be related to the LFH CME if the possible forward shock driven by the ICME decelerates down to the observed solar wind speed downstream this discontinuity (~472 km s^{-1}).

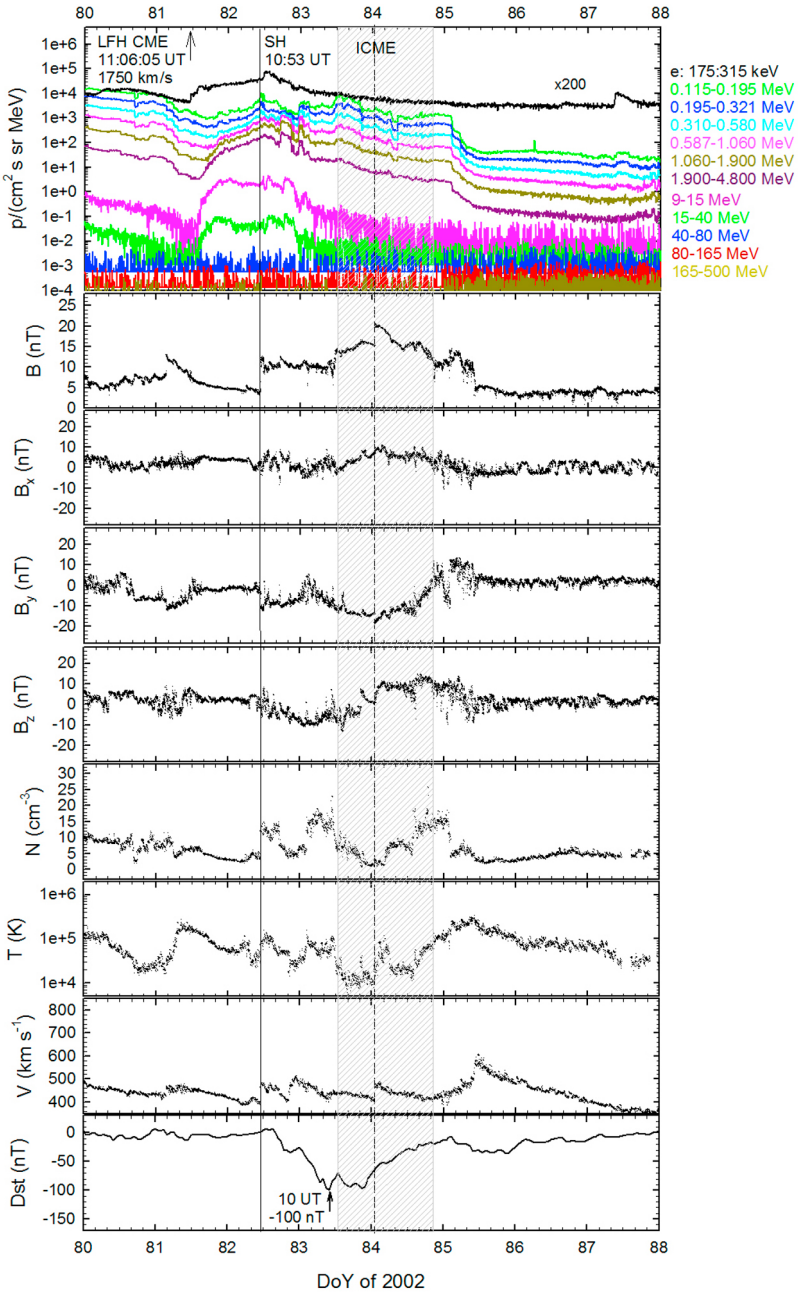

Figure 8. Interplanetary data and *Dst* index for event #11. An arrow in the first panel indicates the time of the first appearance in the field of view of the LASCO/C2 coronagraph of the LFH CME on 22 March 2002. The format is the same as that of Figure 7. The two vertical lines indicate the passage of forward IP shocks by ACE, and the shadowed area corresponds to an ICME passage (see text for details). An arrow in the ninth panel indicates the time of minimum value of the *Dst* index.

Nevertheless, this discontinuity was not geoeffective, according to the *Dst* index and the other indices.

[43] High-energy (10–40 MeV) proton intensities and the 0.175–0.315 MeV electron intensity start to increase shortly after the launch of the LFH CME (Figure 8, first panel). In this case, the SEP flux profiles would be consistent with a western parent activity associated with an IP shock arriving at the time of the discontinuity on 25 March (the same association is given by *Cane et al.* [2006]). However, this relation cannot be made as clearly as for event #9 due to several intervening structures that are present during this SEP event and affect the transport of particles. For instance, just after the IP shock on 23 March, the >0.3 MeV proton flux profiles show a local peak, and they decrease afterward (see Figure 8).

[44] Three days before the occurrence of the LFH CME on 22 March, several widespread CMEs occurred, ranging from PH to HCME angular widths. The first one worth mentioning was the PH CME on 19 March at 09:54 UT, originating from a region right behind the west limb at equatorial latitudes, and

with coronagraph plane-of-sky speed of ~720 km s^{-1}, lacking the characteristics needed to be associated with the disturbance on 23 March. Also on 19 March, at 11:54 UT, a wider PH CME was also observed close to the west limb, this time on the visible side of the Sun, with an apparent speed of ~880 km s^{-1}. Type II radio emission in the range 150–90 kHz is detected by the WAVES TNR receiver in connection to this event. Assuming a local density equal to 7.2 cm^{-3} and that the emission is of the harmonic kind, the shock driven by the latter CME is seen to drift at ~1000 km s^{-1} at a distance of ~0.5 AU. The extrapolation of the shock propagation to 1 AU indicates its arrival at ~19:00 UT on 20 March. Even assuming the emission is of the fundamental kind, the arrival time yields ~01:00 UT on 22 March, still too early to be associated with the in situ signatures discussed here. The next CME takes place on 20 March at 17:54 UT, fully surrounding the coronagraph's occulter in a symmetrical fashion. A weak dimming and a posteruption loop arcade were detected by SOHO/EIT in AR 9871 (S21W15) in association with this white-light event. *Gopalswamy et al.* [2010b] considered this CME on 20 March with the region at S17W20 as a better candidate than the LFH on 22 March for the storm with a minimum on *Dst* on 24 March, previously proposed by *Gopalswamy et al.* [2007] by coincidence. However, there is no obvious activity to assure that that symmetric full halo CME is frontsided; some flares and postflare loops well after the time of the CME without prior dimmings prevent us from performing any unambiguous association. The last plausible candidate, likely responsible for the in situ disturbance beginning on 23 March is the fast PH CME first detected at 23:54 UT on 20 March, traveling with an apparent speed of 1075 km s^{-1}. The complexity exhibited by several active regions close to the west limb and the occurrence of two close dimmings of distinct origin (as seen by EIT in the 195 Å bandpass) do not allow us to establish a one-to-one association. Nevertheless, it can be stated that the CME did originate somewhere close to the west limb, likely involving AR 9866 and AR9870, and maybe interconnected to some region(s) located behind this limb, as indicated by the loop growth observed by EIT 195 Å above the limb. The last two halo events are likely to be responsible for the complex in situ disturbance beginning on 23 March. Therefore, the LFH CME on 22 March is not geoeffective.

4.1.4. Event #21 (14 July 2005)

[45] On 14 July 2005 (DoY 195) at 10:54 UT, a LFH CME appeared in the LASCO C2 coronagraph, originating in AR10786, a highly flare-productive region at N11 on the west limb. A faint type II emission between 135 and 85 kHz (~76–120 R_s assuming a local density of 7.2 cm^{-3}), which traces back to the onset of this LFH CME, suggests the presence of a shock traveling at ~1300 km s^{-1} with an expected arrival time of ~02:00 UT on 16 July 2005.

[46] High-energy (40–80 MeV) protons are seen by GOES-11 in close occurrence with the launch of the LFH CME on 14 July (Figure 9, first panel). This event is clearly separated from a former one most likely associated with a series of solar events developing on 13 July (DoY 194), including a halo CME and three M class X-ray flares at the west limb. Between 9 and 40 MeV, both events can still be differentiated, but they merge in one compound event if lower energies are considered. The ~2 MeV proton intensity profiles show an extended plateau that does not show any relevant increase at the time of the passage of the discontinuity observed in the solar wind plasma on 16–17 July. In fact, at low energies, the absolute peak intensity occurs at ~20:00 UT on 16 July, not coinciding with any of the solar wind discontinuities observed.

[47] Solar wind and IP data are also shown in Figure 9. Two forward shocks were observed by MAG/ACE on 16 July (DoY 197) at 01:50 UT and on 17 July (DoY 198) at 00:55 UT (Figure 9, vertical lines). Another discontinuity in the IMF also appears at 16:00 UT on DoY 197. SWEPAM/ACE observed solar wind discontinuities at the same time in velocity and density data. Temperature is lower upstream than downstream of the first shock, although there is not a clear discontinuity as there is for the last shock. The time of the first discontinuity (16 July at 01:50 UT) is in accordance with the value suggested from type II observations of ~1300 km s^{-1} as stated above.

[48] Several rotations can be seen in the IMF components, between 15:00 UT on DoY 198 and 02:00 UT of the following day, together with the increase and posterior decrease of the field intensity. Combined with a low temperature, these are the indications of a magnetic cloud-type ICME. The flux rope has a NES structure (the magnetic field points toward the north in the leading part of the cloud and to the south in the trailing part, and its internal axis is oriented toward the east). Previous to the rotation, the IMF B_z component remains close to −10 nT for several hours, producing a geomagnetic storm with the *Dst* reaching −67 nT on 18 July (DoY 199) at 07:00 UT. This storm is a double-peak one, with a previous local minimum of −34 nT on 17 July at 11:00 UT. As the *Dst*, all geomagnetic indices are disturbed since ~06:00 UT on 17 July until midday on 18 July (not shown in Figure 9). However, the IP shock on 16 July at 01:50 UT, although noticeable by all indices, cannot be considered a geomagnetic disturbance, as the minimum value of the *Dst* index on 16 July is −21 nT.

[49] There were four events at the Sun that could have caused the transients seen at L1. The first one is a halo CME from 12 July seen first at 16:54 UT on LASCO C2 that could have interacted with a LFH CME from 13 July starting at 14:30 UT, this option would require a large deflection of this CME in order to produce the signatures seen at L1. A second possibility is that the LFH from 14 July overtook the one on the previous day, this would again require large deflection as both CMEs are coming from the W90. A third combination would be given by the CME on 12 July and a CME not observed but marked but dimmings from region S0W47 at 19:13 on 13 July. This last explanation is probably the most likely to have occurred; therefore, we may conclude that the geomagnetic disturbance observed on DoY 199 is not related to the LFH CME.

4.1.5. Event #22 (27 July 2005)

[50] The LFH CME on 27 July 2005 (DoY 208) at 04:54 UT originated from AR10792, located at 12°N on the east solar limb. It was accompanied by a prominence eruption. There is no indication of an Earth-directed shock producing radio type II emission in the Wind/WAVES TNR radio data. All geomagnetic indices are disturbed for a long interval of about 4 days since the end of 27 July (Figure 10, *am* not shown), but the storm can be classified as a minor storm: the *Dst* index reached a peak value of −41 nT on 28 July at

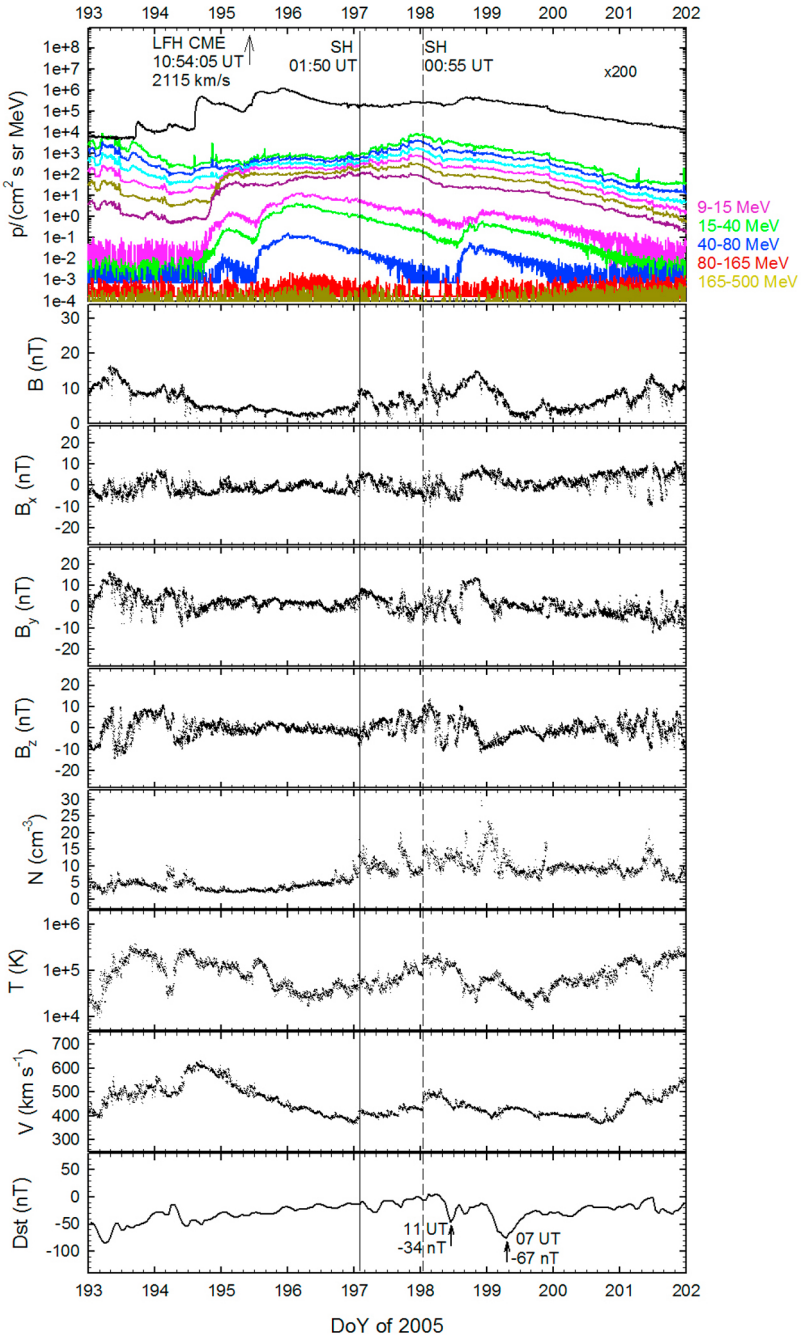

Figure 9. Interplanetary data and *Dst* index for event #21. An arrow in the first panel indicates the time of the first appearance in the field of view of the LASCO/C2 coronagraph of the LFH CME on 14 July 2005). The format is the same as that of Figure 7. The two vertical lines indicate the passage of forward IP shocks by ACE/MAG (see text for details). Arrows in the ninth panel indicate the time of minimum values of the *Dst* index.

06:00 UT, followed by a slow recovery phase of 4 days due to a highly fluctuating magnetic field.

[51] On 27 July, the same day of the LFH CME, an IP discontinuity is observed at ACE at 18:48 UT (Figure 10, solid line) related to the associated *ssc*, ~11 h prior to the *Dst* peak on 28 July. This discontinuity is not a shock driven by the LFH CME because of the short transit time (~14 h) and the small solar wind speed observed downstream of the shock (~400 km s^{-1}). Moreover, it corresponds to a fluctuation in the stream interface between the slow solar wind and the fast one from a coronal hole. Hence, the LFH CME is not the source of the geomagnetic activity observed early on 28 July.

[52] The forward shock observed by ACE at 06:05 UT on 1 August (DoY 213) (Figure 10, dashed line) is most probably driven by the halo CME on 30 July, first seen by

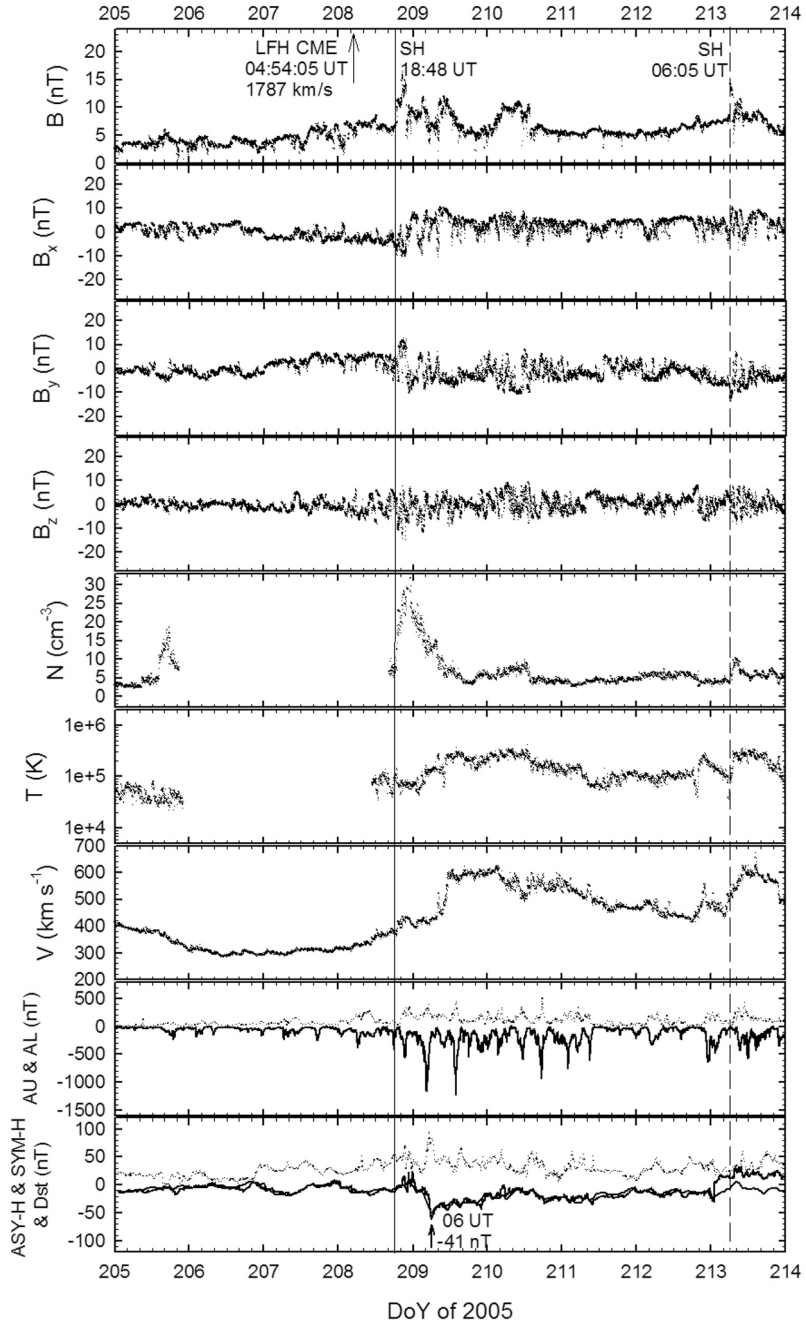

Figure 10. Interplanetary data and geomagnetic indices for event #22. An arrow in the first panel indicates the time of the first appearance in the field of view of the LASCO/C2 coronagraph of the LFH CME on 27 July 2005. Shown, from top to bottom, are the magnetic field intensity and the magnetic field components in GSM coordinates (measured by ACE/MAG); the solar wind density, temperature, and speed (measured by ACE/SWEPAM); the *AU* (dotted line) and *AL* (short dashed line) geomagnetic indices; and the *Dst* (solid line), *SYM-H* (short dashed line), and *ASY-H* (dotted line) indices. The arrow in the ninth panel marks the time of minimum value of the *Dst* index. The two vertical lines indicate the passage of forward IP shocks by ACE.

LASCO at 06:50 UT. This halo CME had a plane-of-sky speed of 1968 km s^{-1}, and it is in temporal association with an X1.3 flare starting at 06:17 UT and originating from N12E60 [see also *Gopalswamy et al.*, 2010b]. However, this IP shock did not disturb the terrestrial environment, as seen by the indices analyzed. The observed geoeffectiveness starting late on 27 July (DoY 208) is due to the effect of a fast solar wind stream observed from 28 July at ~01:30 UT to 31 July (DoY 212) at ~05:30 UT. The decrease on the *SYM-H* and *Dst* geomagnetic indices takes place due to a

small southern IMF interval in the interface between slow and fast solar wind.

[53] From 24 to 27 July, there were five halo CMEs with projected speeds >1200 km s^{-1} moving out from the east limb. The source of all of them, but that on 27 July, was backsided. The two fastest were the CMEs originating on 24 July at 13:54 UT (2528 km s^{-1}) and on 25 July at 11:06 UT (1660 km s^{-1}). The 15–40 MeV proton intensities recorded by GOES-11 start to increase just after the occurrence of the latter halo CME, but protons at lower energies (<5 MeV) were already above background levels at that time, indicating a previous source of particles. Moreover, the presence of type II radio emission indicates the existence of a shock plausibly associated with the halo CME on 24 July and not with the halo CME on 25 July. Hence, the driver of the IP shock seen on 28 July at 18:48 UT was most probably the first halo CME from the limb. Using type III radio data, Cane *et al.* [2006] identified the E110 flare at 13:45 on 24 July, as the associated solar origin location of the SEP event. This flare is temporally related to the halo CME on 24 July. Cane *et al.* [2006] also indicate that this SEP event is associated with the shock seen at 1 AU on 28 July. Consequently, the LFH CME on 27 July was not the source of the geoeffectiveness on 28 July.

4.1.6. Event #25 (25 January 2007)

[54] The LFH CME on 25 January 2007 (DoY 25) at 06:54 UT originated from AR10940 at 6° South S08 on the Sun's east limb. Its inferred plane-of-sky speed is 1367 km s^{-1}. This CME is associated with a C6.3 flare, peaking at 07:14 UT and located at S08E90. The Wind/WAVES detectors registered type II emission drifting down from 14,000 to 90 kHz. The slope of this drifting emission suggests a speed of ∼1030 km s^{-1} along the range ∼27–67 R_s and assuming, in this case, a local plasma frequency at Wind of 10 cm^{-3}, given that the local electronic plasma frequency line was quite stable around that value during the days 25–27 January. Assuming this speed is kept constant and that the shock reaches Wind, the inferred estimated arrival would take place on Feb. 27, at ∼01:00 UT. Analysis of the shock evolution at higher frequencies (i.e., closer to the Sun) can be found in Gopalswamy *et al.* [2009b].

[55] All geomagnetic indices are quiet for a long interval of about 4 days since the beginning of 25 January, followed by clear activity on all indices since midday of 29 January until the end of the 5 day period considered (Figure 11, *am* not shown). The storm can be classified as a minor storm: the *Dst* index reached a peak value of −49 nT on 29 January at 22:00 UT (more than 4 days after the appearance of the LFH CME in the LASCO C2 coronagraph). The observed geoeffectiveness is due to the effect of a fast solar wind stream observed from 29 January at ∼19:20 UT and the interaction region between fast and slow previous solar wind (Figure 11, shadowed area). Hence, the LFH CME is not the source of the geomagnetic activity observed on 29 January.

4.2. LFH CMEs Associated With a Geomagnetic Disturbance

[56] In this section, we discuss the geoeffective events where the LFH CME can be related to the geoeffectiveness. We distinguish the cases whether the LFH CME is the cause of the geoeffectiveness or if it could enhance the disturbance produced by other solar ejections.

4.2.1. Event #7 (1 October 2001)

[57] The solar source of the LFH CME on 1 October (DoY 274) at 05:30 UT was AR 9628 at S18W90. The observed type II radio burst on the same day in the Wind/WAVES RAD1 data suggests an IP shock traveling at ∼850 km s^{-1} across a heliocentric distance of 13–52 R_s (∼800–200 kHz), assuming n_e = 7.2 cm^{-3} at Wind [see also *Gopalswamy et al.*, 2004]. ACE observed an IP shock on 3 October (DoY 276) at 08:00 UT (Figure 12, dashed line). Assuming that the driving ICME results from the LFH CME observed at 05:30 UT on DoY 274 [see *Cane et al.*, 2010, Table 1], a transit time from the Sun to the Earth of ∼48 h and an average speed of 860 km s^{-1} are inferred. The latter value is similar to the speed derived from the type II emission profile at distances of 13–52 R_s. This coincidence may be regarded as an indication of the shock traveling across those distances at the average speed value, while it may slow down further at larger distances. At the same time, it is reasonable to interpret that the similarity exists because this emission takes place at a portion of the shock traveling toward Earth, i.e., the flank. Back to ACE, downstream of the IP shock, a southern IMF of approximately −20 nT lasting more than 5 h is responsible for the decrease of an already disturbed *Dst* index to a peak value of −166 nT.

[58] SEP intensities at high energy (from ∼2 to ∼80 MeV) show an enhancement about 4 h after the CME launch, with a second increase due to the passage of the shock on DoY 276 (Figure 12, dashed line). Although the particle onset takes place in a perturbed solar wind/IMF regime due to another former IP shock (Figure 12, solid line), which in turn can be one reason for the delay of the onset of the event, the evolution of these particle profiles suggests that this driven shock is associated with the LFH CME on DoY 274, because the proton flux profiles at all energies are consistent with this interpretation. ACE observed the passage of this shock about 10 h before the launch of the LFH CME. There is the possibility that the associated interplanetary structure modified the IMF. If this has been the case, the magnetic connection between the LFH CME-driven shock and the ACE spacecraft is not as simple as expected from the Parker spiral of a nonperturbed solar wind of ∼500 km s^{-1}.

[59] In the upstream region of the IP shock on DoY 276 at 8:00 UT, the IMF shows northern polarity, and it is enhanced to ∼10 nT until about 3 h before the shock arrival when it turns smoothly southern. The smoothness of the IMF together with a decreased proton temperature and a ratio of alphas to protons up to ∼0.5 (not shown in Figure 12), clearly above background, indicate the presence of a previous ICME. This ICME, the signatures of which start on 3 October at ∼00:00 UT, does not drive any shock (in fact, it travels slower than the solar wind ahead). Proton temperature slightly increases after the shock passage at about 8 h later, and it remains depleted during the following 8 h. Then, temperature sharply increases, indicating the rear boundary of the ICME. There is also a remarkable jump in the magnetic field due to the IP shock, which induces a not negligible compression of the magnetic field of the previous ICME. To explain these solar wind and IMF features, we propose the following scenario: during its journey to ACE and Earth, the IP shock encounters and overtakes a former ICME most probably produced near the central meridian, as the PH CME observed on 29 September at 11:54:05 UT

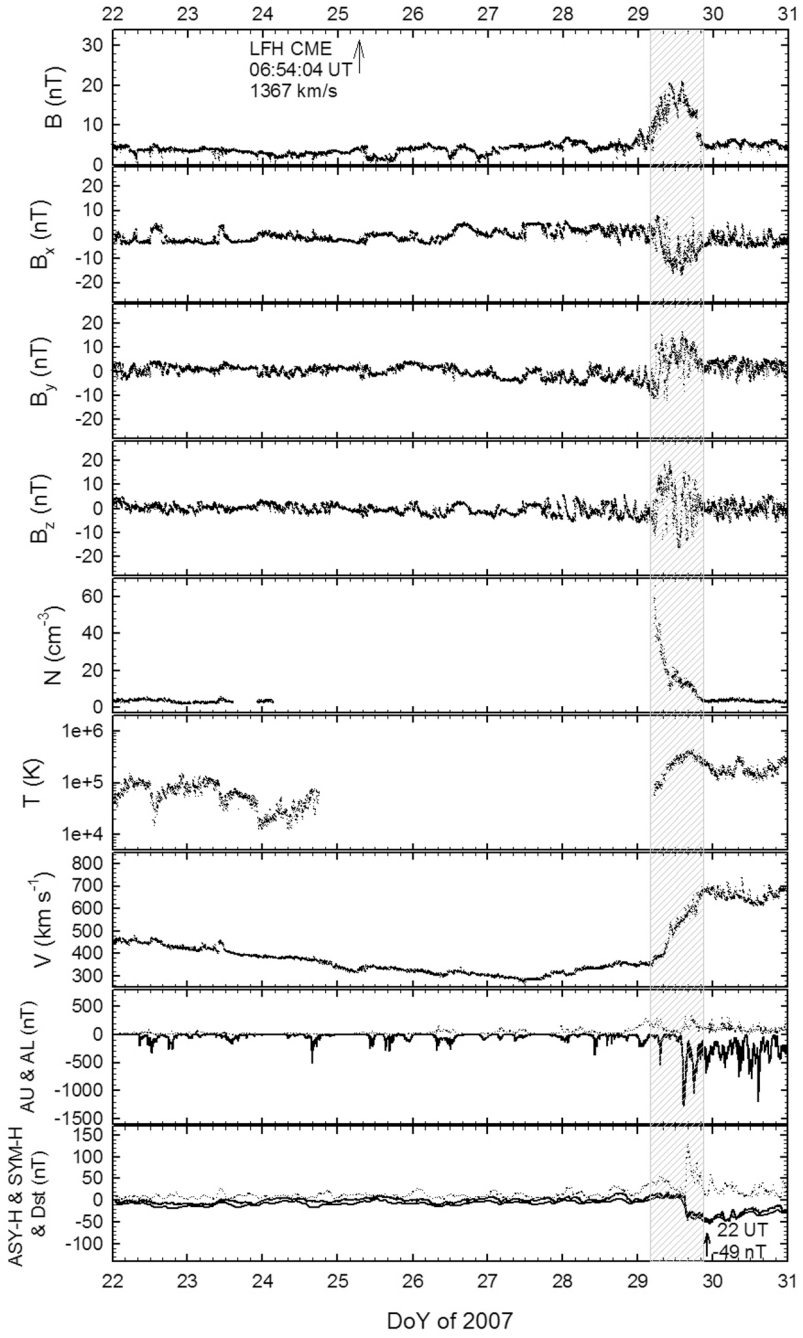

Figure 11. Interplanetary data and geomagnetic indices for event #25. An arrow in the first panel indicates the time of the first appearance in the field of view of the LASCO/C2 coronagraph of the LFH CME on 25 January 2007. The format is the same as that of Figure 10. The shadowed area indicates the interaction region between the fast stream and the slow solar wind. An arrow in the ninth panel marks the time of minimum value of the *Dst* index.

(likely in AR9636). Wind/WAVES cannot shed light on this possibility due to the difficulty to discern radio bursts in times of such elevated solar activity.

[60] Besides the uncertainty of the identification of the ICME solar parent event, several features described above indicate a relationship between the IP shock on 3 October observed by ACE at 08:00 UT and the LFH CME. Therefore, although the previous ICME provides the negative B_z related to the initial decrease of the *Dst* index (after the increase related to the associated *ssc*), it is the IP shock related to the LFH CME that produces a strong jump in the IMF and, consequently, in southern B_z, finally developing an intense storm with a peak value of −166 nT. However, the *Dst* index was recovering from a previous geomagnetic storm with values ranging between −80 and −100 nT on 2 October. In short, we conclude that the LFH CME on 1 October is geoeffective.

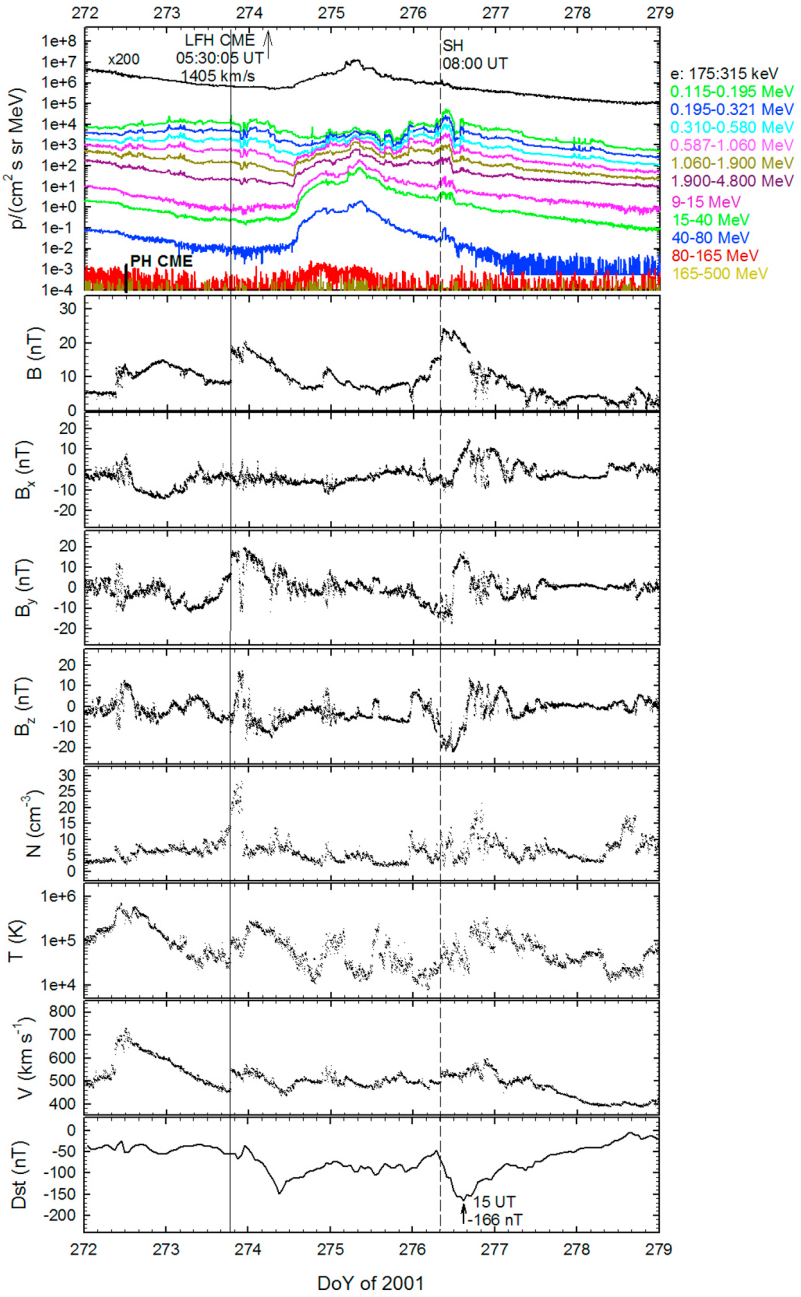

Figure 12. Interplanetary data and *Dst* index for event #7. An arrow in the first panel indicates the time of first appearance in the field of view of the LASCO/C2 coronagraph of the LFH CME on 1 October 2001. The format is the same as that of Figure 7. The two vertical lines indicate the passage of forward IP shocks by ACE (see text for details). An arrow in the ninth panel marks the time of minimum value of the *Dst* index.

4.2.2. Event #12 (21 April 2002)

[61] This limb full halo CME is first identified in the LASCO C2 coronagraph at 01:27 UT on 21 April 2002 (DoY 111), at equatorial latitudes on the west limb, and later on it develops into a full halo CME observed in the FOV of LASCO C3. During an eruption in AR 09906 observed at 01:13 UT in EIT 195 Å, GOES detected a large X1.5 flare at S14W84. This event was previously reported, among others, by *Gopalswamy et al.* [2010b]. This eruption triggered at 02:00 UT the lift off of a nearby quiescent filament, whose presence is evidenced somewhat later within the fine structure of this CME. A linear fit through the height-time points taken by the LASCO CME catalog's operator yields a plane-of-sky speed of ~2400 km s^{-1}.

[62] The ACE data for this event are shown in Figure 13. As can be seen, an IP shock (Figure 13, solid line) is observed at 04:00 UT on 23 April (DoY 113), producing a sudden impulse in the *Dst* index. Following the shock, a sheath region can be identified by the high temperatures and densities and by the compressed magnetic field observed in this region. *Dst* values start decreasing significantly in this sheath region, because it contains a negative B_z structure with values

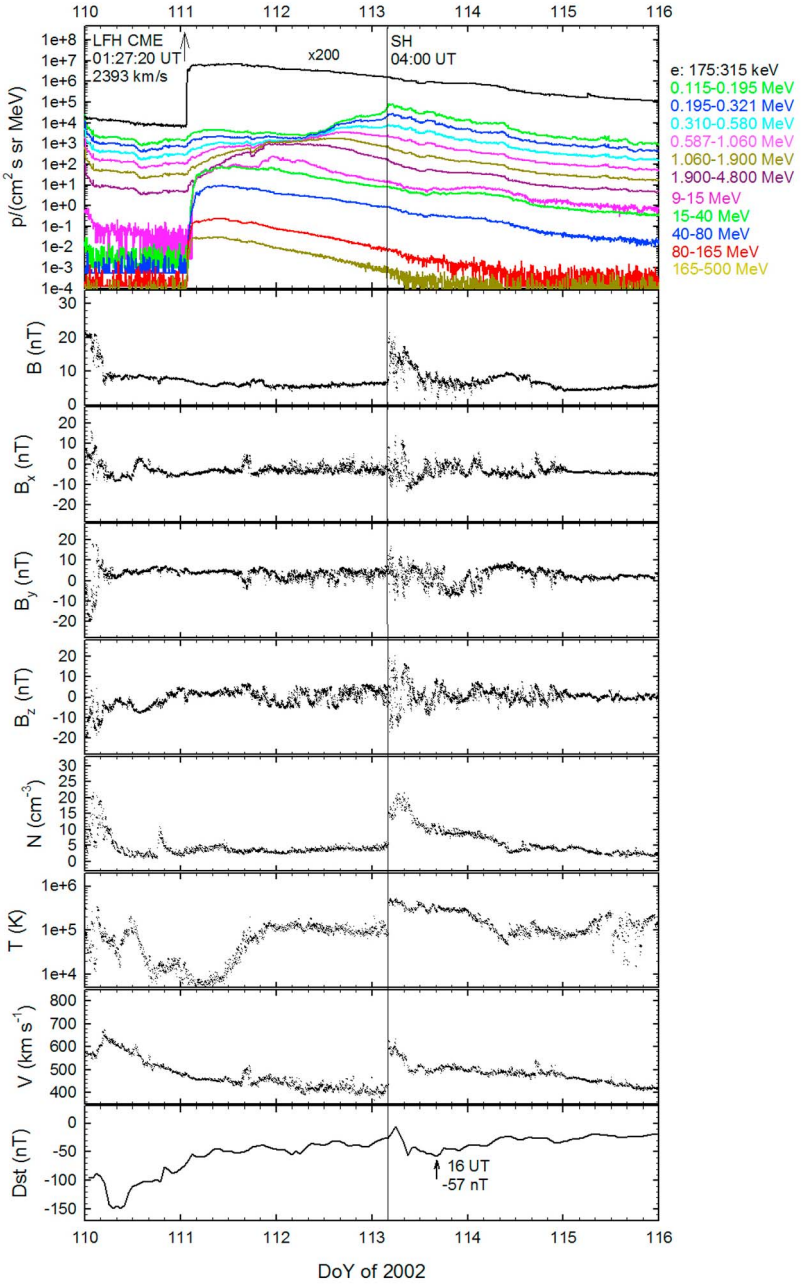

Figure 13. Interplanetary data and *Dst* index for event #12. An arrow in the first panel indicates the time of first appearance in the field of view of the LASCO/C2 coronagraph of the LFH CME on 21 April 2002. The format is the same as that of Figure 7. The two vertical lines indicate the passage of forward IP shocks by ACE (see text for details). An arrow in the ninth panel marks the time of minimum value of the *Dst* index.

reaching −16 nT. This causes a moderate geomagnetic storm with a *Dst* reaching −57 nT on 23 April at 16:00 UT. There are no signatures of the ejecta itself, which most probably passed to the west of the Earth.

[63] Wind/WAVES TNR data show kilometric type II emission after this LFH CME, whose slope was measured between the range 110–50 kHz (∼35–75 R_s from the Sun). The latter indicates a traveling speed of ∼800 km s^{-1} (Figure 14), assuming, in this case, a local plasma frequency at Wind of 4 cm^{-3}, given that the local electronic plasma frequency line was quite stable around that value. The expected arrival time to 1 AU almost coincides with that of the shock detected by ACE, which supports their association.

[64] High-energy (>80 MeV) protons are observed shortly after the X-ray flare eruption. The smooth change in shape of the proton intensity-time profiles from high energy, peaking at the prompt phase, to low energies (<0.5 MeV), peaking at the shock passage, strongly supports that the IP shock observed corresponds to the LFH CME observed on DoY 111.

4.2.3. Event #16 (15 June 2003)

[65] The LFH CME on 15 June 2003 (DoY 166) first appeared in LASCO C2 at 23:54 UT, arising from AR10386

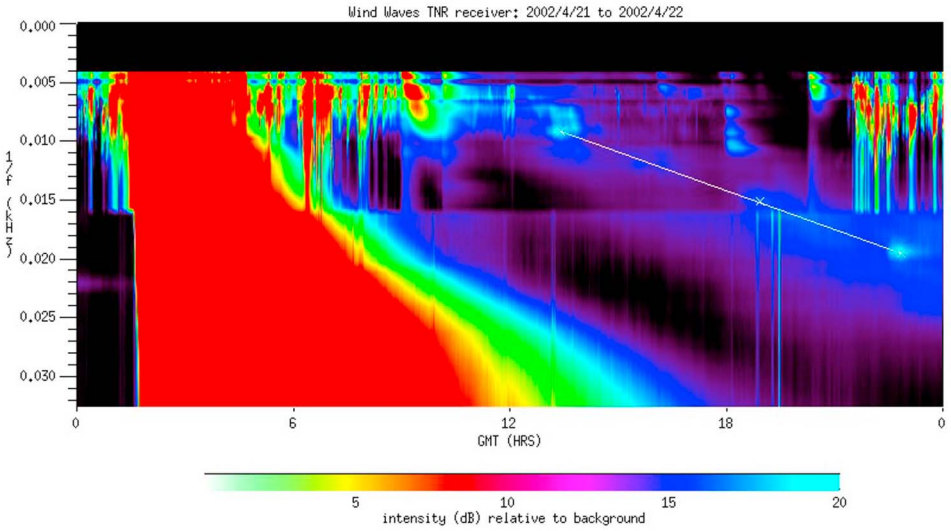

Figure 14. Type II emission related to the LFH CME on 21 April 2002 as observed in the Wind/WAVES dynamic spectrum. The slope of the emission drifting down in frequency indicates an IP shock traveling at ~800 km s^{-1} with an estimated arrival time almost coincident with that of the shock arrival at ACE.

at S07 on the Sun's east limb. Its inferred plane-of-sky speed is 2053 km s^{-1}. This CME is associated with an X1.3 flare, peaking at 23:56 UT and located at S07E80. According to the Wind/WAVES TII listing and the type II catalog at the CDAW data center, the type II emission reported on 16 June 2003 reaches 400 kHz. However, a kilometric smoothly downward drifting feature was found in the WAVES/TNR data. Its travel speed around 0.5 AU (73–53 kHz) was derived to be 530 km s^{-1}, assuming a local plasma density of 11.5 cm^{-3} and an emission at the fundamental component. Propagating at a constant speed from this point onward, its arrival would be expected to occur at ~09:00 UT on 18 June. For E<40 MeV, proton intensities simultaneously increase immediately after the passage of a solar wind and magnetic field discontinuity at 08:45 UT on 18 June (DoY 169) (dashed line in Figure 15). The simultaneous particle increase suggests that particles have been locally trapped by a magnetic barrier and their enhancement is only observed after the discontinuity has swept the spacecraft. Such situations have been formerly studied at low (<4 MeV) [*van Nes et al.*, 1985] and high energies [*Lario et al.*, 2008]. This small SEP event is likely associated with the HCME on 17 June at 23:18 UT, but there might be a contribution at low energy from the LFH CMEs downstream.

[66] Nevertheless, the same day at 04:28 UT, ACE detected another discontinuity in the solar wind speed and in the magnetic field intensity (Figure 15, solid line); this is just ~5 h prior to the *Dst* peak. This discontinuity or shock can be confirmed by solar wind density and temperature jumps from ACE/SWEPAM 64-s level 2 data. Note that the proton monitor sensor of SOHO/CELIAS/MTOF/instrument [*Ipavich et al.*, 1998] detected a shock at 04:44 UT that same day (http://umtof.umd.edu/pm). This shock occurs about 52 h after the LFH CME was first seen by LASCO. *Cane et al.* [2010] and Gopalswamy *et al.* [2010b, 2010d] associated this shock with the LFH CME observed by LASCO on 15 June at 23:54 UT.

[67] Between the more than 4 h interval between both discontinuities, the alpha-to-proton density ratio is clearly enhanced over the background. Moreover, the GSM magnetic field z-component is steady and southern with values approximately –20 nT. As a consequence, the *Dst* index, which already exhibited a decreasing time profile since DoY 167 at 10:00 UT, decreased again from −51 nT at 06:00 UT to −141 nT at 10:00 UT. *Astafyeva* [2009] studied the ionospheric effects of this geomagnetic storm and also comments that its source is related to the shock driven by the LFH CME.

4.2.4. Event #17 (4 November 2003)

[68] This LFH CME appeared in the field of view of LASCO C2 at 19:54 UT on 4 November (DoY 308), after an X17 flare (the largest of our list) at S19W83 within AR10486. The plane-of-sky projected speed as measured from both LASCO coronagraphs yielded ~2650 km s^{-1}. ACE observed an IP shock on 6 November (DoY 310) at 19:19 UT (Figure 16, solid line). Type II emission present in Wind/WAVES data, indicates an IP shock undoubtedly related to the LFH CME. Its slope was derived from the profile evident in the RAD1 dynamic spectrum, within the range 700–90 kHz (~6.5–40 R_s) from the Sun. It indicates a traveling speed of ~930 km s^{-1} (Figure 17), assuming, in this case, a local plasma frequency at Wind of 4 cm^{-3}, given that the local electronic plasma frequency line was quite stable around that value. Assuming constant speed and an earthward propagation of the emitting portion of the shock, its estimated arrival time is 6 November at 17:00 UT, thus indicating a likely association. This event was previously reported, among others, by *Gopalswamy et al.* [2010b].

[69] First high-energy (>80 MeV) protons detected by GOES-11 at 1 AU were released at the time of the X-ray flare (after correcting the flight time along the IMF), with particle intensities peaking shortly after, at the prompt phase (Figure 16, first panel). Low-energy (<5 MeV) proton profiles observed by ACE/EPAM have high pre-event intensities due to a previous large SEP event on 2 November. These low-energy profiles peak at the shock arrival. The high-to-low energy set of flux profiles strongly suggest that the shock on 6 November corresponds to the LFH CME

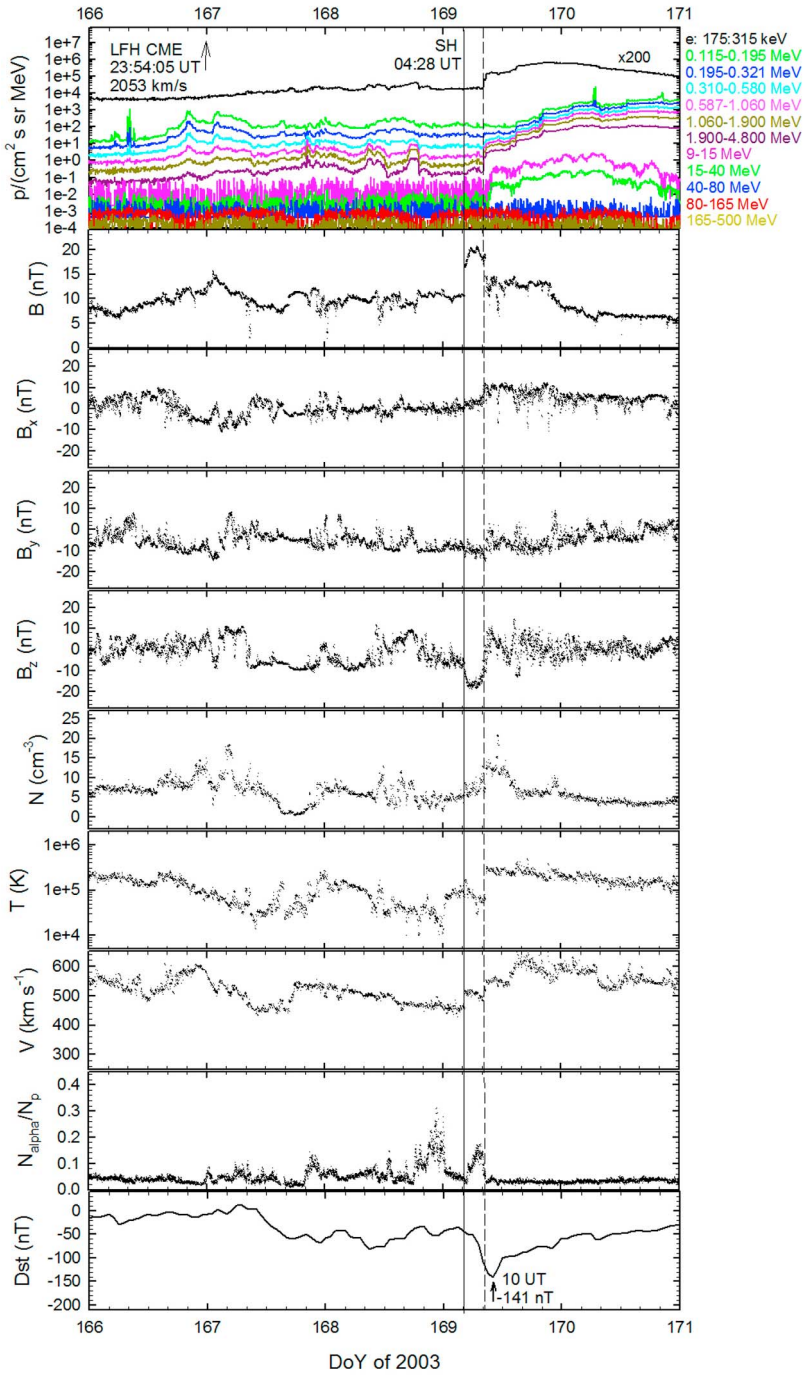

Figure 15. Interplanetary data and *Dst* index for event #16. An arrow in the first panel indicates the time of the first appearance in the field of view of the LASCO/C2 coronagraph of the LFH CME on 15 June 2003. The first panel shows proton intensity-time profiles measured by the ACE/EPAM/LEMS120 detector, from 0.115 to 4.8 MeV (color coded). The black trace corresponds to the 115–315 keV electron intensity measured by the ACE/EPAM/DE30 detector, multiplied by 200 as indicated. Shown, from top to bottom, are the magnetic field intensity and the magnetic field components in GSM coordinates (measured by ACE/MAG); the solar wind density, temperature, and speed; and the alpha-to-proton density ratio (measured by ACE/SWEPAM). The two vertical lines indicate the passage of discontinuities by ACE (see text for details). The tenth panel shows the *Dst* index. An arrow in the tenth panel indicates the time of minimum value of the *Dst* index.

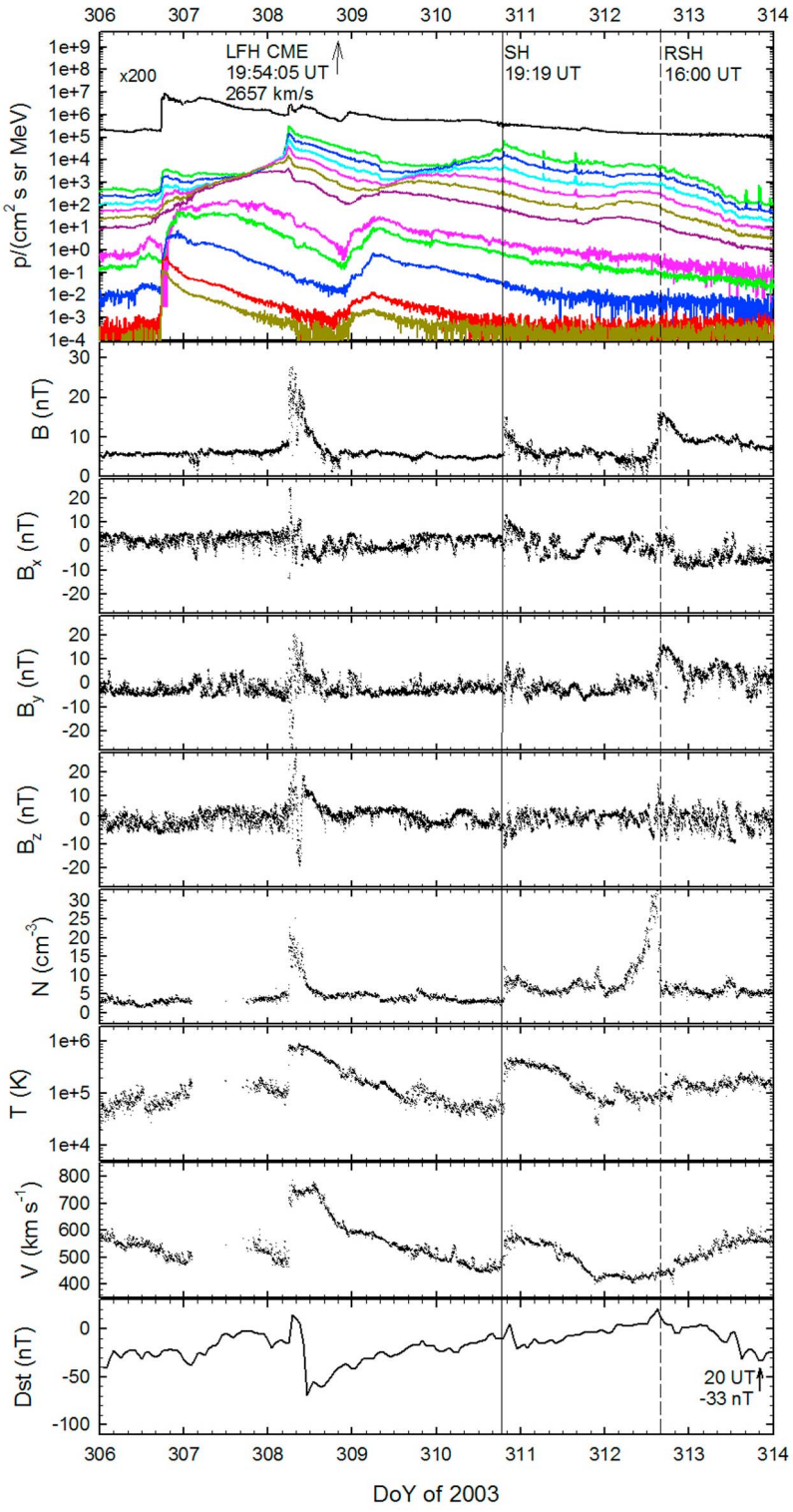

Figure 16. Interplanetary data and *Dst* index for event #17. An arrow in the first panel indicates the time of the first appearance in the field of view of the LASCO/C2 coronagraph of the LFH CME on 4 November 2003. The format is the same as that of Figure 7. The two vertical lines indicate the passage of IP shocks by ACE (see text for details). An arrow in the ninth panel indicates the time of minimum value of the *Dst* index.

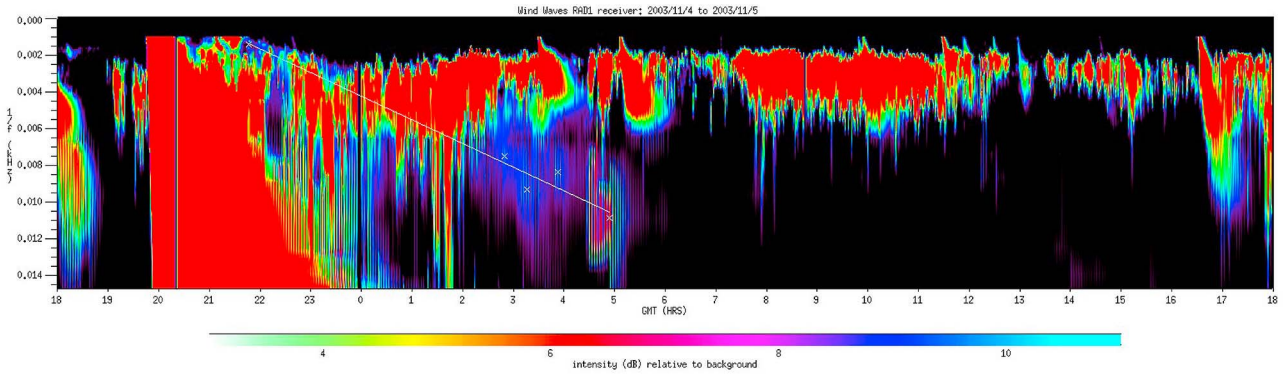

Figure 17. Type II emission related to the LFH CME on 4 November 2003 as observed in the Wind/WAVES dynamic spectrum. The slope of the emission drifting down in frequency indicates an IP shock traveling at ~930 km s^{-1} with an estimated arrival time on 6 November at ~17:00 UT. The linear fit is calculated from the white crosses pinpointing the emission patches.

observed on DoY 308, supporting the association made from radio data.

[70] As a consequence of this IP shock and the southern magnetic field observed downstream, geomagnetic indices *AU* and *AL* show that the terrestrial magnetosphere is disturbed at high latitudes on 6 November (DoY 310). *ASY-H* shows a large disturbance over the background that is also registered at the planetary level, as indicated by the disturbed *am* index (see Figure 5). Although neither *SYM-H* nor *Dst* values surpass the threshold of −50 nT, these indices, which recover from a previous event in the beginning of the interval analyzed, show an increase at around 21:00 UT corresponding to an *ssc*, already reported by *Gopalswamy et al.* [2005b]. After this time, there is a clear decrease in the *Dst* from +5 to −21 nT at 23:00 UT followed by a slow recovery phase. A new disturbance is observed starting late on 8 November (DoY 312) that reaches a peak value of −33 nT on 9 November at 20:00 UT. The peak value has a lower value than the previous one, hence it has been included in Table 1. However, this disturbance is related to a reverse shock that clearly appears in the magnetic field intensity and in the solar wind density at about 16:00 UT (Figure 16, dashed line) and therefore is not associated with the LFH CME.

[71] In summary, the IP shock observed on 6 November is related to the LFH CME that disturbs the magnetosphere at all latitudes and at the planetary level, although the *Dst* and *SYM-H* indices did not fall below the −50 nT threshold.

5. Summary and Conclusions

[72] Of the 25 LFH CME events identified in solar cycle 23, only 10 events show signatures of disturbance of the terrestrial environment between 1 and 5 days after the CMEs' first appearances in LASCO/C2. After a careful analysis of solar, interplanetary, and terrestrial data, we conclude that four of them are geoeffective LFH CMEs: the events on 1 October 2001, 21 April 2002, 15 June 2003, and 4 November 2003.

[73] The 1 October 2001 and the 15 June 2003 events generated intense storms, with the *Dst* index peaking well below −100 nT (−166 and −141 nT, respectively). The high disturbance they induced is related to the preconditioning of the magnetosphere, already disturbed by a previous event. Therefore, these LFH CMEs enhanced the geoeffectiveness led by preceding events.

[74] The LFH on 21 April 2002 produced a moderate storm, Dst_{min} = −57 nT. The 4 November 2003 event was related to disturbances at high-latitude regions (as identified from the *AU* and *AL* indices), and it was observed at the planetary level (as indicated by the disturbed *am* index); nevertheless, it was nongeoeffective at *Dst* index values.

[75] Through the analysis of the five geoeffective intervals where the LFH CME was not related to the disturbance, we have been able to derive that the solar source related to the geoeffectiveness was close to the west limb in three cases (23 April 1989, 22 March 2002, and 14 July 2005), or even backsided for the event on 27 July 2005. Only in one case (28 December 2001) was the solar source not close to the limb, but on W54. All those geomagnetic storms were moderate, except that on 22 March 2002, for which the *Dst* index reached −100 nT. This large disturbance from a solar location far from the central solar meridian could be due to the fact that the ejection arose from the interaction between two active regions, supporting the results by *Cerrato et al.* [2012].

[76] On the basis of the events analyzed, we conclude that LFH CMEs are able to disturb the terrestrial environment. We have not found any evidence for intense or severe geomagnetic storms associated only with a LFH CME; to produce an intense disturbance, it is necessary to have the magnetosphere already preconditioned by a previous solar ejection. In this case, an intense storm arises. Nevertheless, solar ejections from the interaction between two active regions close to the west limb have been found to be associated with an intense storm.

[77] A three-point view of the Sun, as provided by the STEREO and SOHO spacecraft, was not available during solar cycle 23, and therefore the determination of the solar sources of geomagnetic events was not always a straightforward process. Type II emission and energetic particles were key to establish the whole Sun-Earth chain of the analyzed events.

[78] **Acknowledgments.** The authors thank the International Space Science Institute (Bern, Switzerland) for supporting the project "From the Sun to the terrestrial surface: understanding the chain," led by C. Cid, and all data sources used in this work. This work was supported by the Spanish projects PN-AYA 2007-60724, PN-AYA2009-08662, and PN-AYA2010-

17286 from the Ministerio de Ciencia e Innovación and PPII10-0183-7802 from the Junta de Comunidades de Castilla-La Mancha of Spain and by the French project PNST/GMI 2008–2011 (Group of multi-instruments). B.Sa. also acknowledges the computational support provided by the Centre de Serveis Científics i Acadèmics de Catalunya (CESCA). A.A. acknowledges the support of an ESA internal research fellowship. S.D. acknowledges partial support from the Abdus Salam International Centre for Theoretical Physics (ICTP), as provided in the frame of his regular associateship, and from the Universidad de Buenos Aires (grant UBACyT 20020090100264). L.R. and A.Z. acknowledge support from the Belgian Federal Science Policy Office through the ESA-PRODEX program. The present work has received funding from the European Union Seventh Framework Programme (FP7/2007–2013) under grant agreement 263252 [COMESEP]. C.J. gratefully acknowledges support from FWO-Vlaanderen. A.A., B.Sa., C.C., E.S., and Y.C. are members of the COST Action ES0803. H.C., C.M., and S.D. are members of the Carrera del Investigador Científico, CONICET.

[79] Philippa Browning thanks two anonymous reviewers for assistance evaluating this paper.

References

Agueda, N., D. Lario, R. Vainio, B. Sanahuja, E. Kilpua, and S. Pohjolainen (2009), Modeling solar near-relativistic electron events. Insights into solar injection and interplanetary transport conditions, *Astron. Astrophys.*, *507*, 981–993, doi:10.1051/0004-6361/200912224.

Anonymous (2005), The last word: The definition of halo coronal mass ejections, *Eos Trans. AGU*, *86*(30), 281–282, doi:10.1029/2005EO300005.

Astafyeva, E. (2009), Effects of strong IMF Bz southward events on the equatorial and mid-latitude ionosphere, *Ann. Geophys.*, *27*, 1175–1187, doi:10.5194/angeo-27-1175-2009.

Bothmer, V., and A. Zhukov (2007), The Sun as a prime source of space weather, in *Space Weather—Physics and Effects*, pp. 31–102, Springer Praxis Books, Berlin, doi:10.1007/978-3-540-34578-7_3.

Bougeret, J.-L., et al. (1995), Waves: The Radio and Plasma Wave Investigation on the Wind Spacecraft, *Space Sci. Rev.*, *71*, 231–263, doi:10.1007/BF00751331.

Burlaga, L. F., S. P. Plunkett, and O. C. St. Cyr (2002), Successive CMEs and complex ejecta, *J. Geophys. Res.*, *107*(A10), 1266, doi:10.1029/2001JA000255.

Cane, H. V., and I. G. Richardson (2003), Interplanetary coronal mass ejections in the near-Earth solar wind during 1996–2002, *J. Geophys. Res.*, *108*(A4), 1156, doi:10.1029/2002JA009817.

Cane, H. V., R. A. Mewaldt, C. M. S. Cohen, and T. T. von Rosenvinge (2006), Role of flares and shocks in determining solar energetic particle abundances, *J. Geophys. Res.*, *111*, A06S90, doi:10.1029/2005JA011071.

Cane, H. V., I. G. Richardson, and T. T. von Rosenvinge (2010), A study of solar energetic particle events of 1997–2006. Their composition and association, *J. Geophys. Res.*, *115*, A08101, doi:10.1029/2009JA014848.

Cerrato, Y., E. Saiz, C. Cid, W. D. Gonzalez, and J. Palacios (2012), Solar and interplanetary triggers of the largest Dst variations of solar cycle 23, *J. Atmos. Sol. Terr. Phys.*, doi:10.1016/j.jastp.2011.09.001, in press.

Davis, T. N., and M. Sugiura (1966), Auroral electrojet activity index *AE* and its universal time variations, *J. Geophys. Res.*, *71*(3), 785–801, doi:10.1029/JZ071i003p00785.

Dasso, S., et al. (2009), Linking two consecutive nonmerging magnetic clouds with their solar sources, *J. Geophys. Res.*, *114*, A02109, doi:10.1029/2008JA013102.

Delaboudinière, J.-P., et al. (1995), EIT: Extreme-Ultraviolet Imaging Telescope for the SOHO Mission, *Sol. Phys.*, *162*, 291–312, doi:10.1007/BF00733432.

Dere, K. P., and P. Subramanian (2001), Source regions of coronal mass ejections, in *Recent Insights into the Physics of the Sun and Heliosphere: Highlights from SOHO and Other Space Missions, Proceedings of IAU Symposium 203*, edited by P. Brekke, B. Fleck, and J. B. Gurman, pp. 362–373, Astronom. Soc. of the Pacific, San Francisco, Calif., ISBN: 1-58381-069-2.

Gold, R. E., et al. (1998), Electron, proton and alpha monitor on the advanced composition explorer spacecraft, *Space Sci. Rev.*, *86*, 541–562, doi:10.1023/A:1005088115759.

Gonzalez, W. D., J. A. Joselyn, Y. Kamide, H. W. Kroehl, G. Rostoker, B. T. Tsurutani, and V. M. Vasyliunas (1994), What is a geomagnetic storm? *J. Geophys. Res.*, *99*(A4), 5771–5792, doi:10.1029/93JA02867.

Gonzalez, W. D., B. T. Tsurutani, and A. L. C. Gonzalez (1999), Interplanetary origin of geomagnetic storms, *Space Sci. Rev.*, *88*, 529–562, doi:10.1023/A:1005160129098.

Gopalswamy, N. (2002), Relation between coronal mass ejections and their interplanetary counterparts, in *Proceedings of the COSPAR Colloquium*, *COSPAR Colloquia Ser.*, vol. 14, 1st ed., edited by H. Wang and R. Xu, pp. 157–164, Pergamon, Boston.

Gopalswamy, N. (2010), The CME link to geomagnetic storms, in *Solar and Stellar Variability: Impact on Earth and Planets, Proceedings of the International Astronomical Union, IAU Symposium*, vol. 264, pp. 326–335, Cambridge Univ. Press, Cambridge, U. K.

Gopalswamy, N., A. Lara, M. L. Kaiser, and J.-L. Bougeret (2001), Near-Sun and near-Earth manifestations of solar eruptions, *J. Geophys. Res.*, *106*(A11), 25,261–25,277, doi:10.1029/2000JA004025.

Gopalswamy, N., S. Yashiro, A. Lara, M. L. Kaiser, B. J. Thompson, P. T. Gallagher, and R. A. Howard (2003), Large solar energetic particle events of cycle 23: A global view, *Geophys. Res. Lett.*, *30*(12), 8015, doi:10.1029/2002GL016435.

Gopalswamy, N., S. Yashiro, S. Krucker, G. Stenborg, and R. A. Howard (2004), Intensity variation of large solar energetic particle events associated with coronal mass ejections, *J. Geophys. Res.*, *109*, A12105, doi:10.1029/2004JA010602.

Gopalswamy, N., E. Aguilar-Rodriguez, S. Yashiro, S. Nunes, M. L. Kaiser, and R. A. Howard (2005a), Type II radio bursts and energetic solar eruptions, *J. Geophys. Res.*, *110*, A12S07, doi:10.1029/2005JA011158.

Gopalswamy, N., S. Yashiro, Y. Liu, G. Michalek, A. Vourlidas, M. L. Kaiser, and R. A. Howard (2005b), Coronal mass ejections and other extreme characteristics of the 2003 October–November solar eruptions, *J. Geophys. Res.*, *110*, A09S15, doi:10.1029/2004JA010958.

Gopalswamy, N., S. Yashiro, and S. Akiyama (2007), Geoeffectiveness of halo coronal mass ejections, *J. Geophys. Res.*, *112*, A06112, doi:10.1029/2006JA012149.

Gopalswamy, N., S. Yashiro, G. Michalek, G. Stenborg, A. Vourlidas, S. Freeland, and R. Howard (2009a), The SOHO/LASCO CME catalog, *Earth Moon Planets*, *104*, 295–313, doi:10.1007/s11038-008-9282-7.

Gopalswamy, N., W. T. Thompson, J. M. Davila, M. L. Kaiser, S. Yashiro, P. Mäkelä, G. Michalek, J.-L. Bougeret, and R. A. Howard (2009b), Relation between type II bursts and CMEs inferred from STEREO observations, *Sol. Phys.*, *259*, 227–254, doi:10.1007/s11207-009-9382-1.

Gopalswamy, N., S. Yashiro, G. Michalek, H. Xie, P. Mäkelä, A. Vourlidas, and R. A. Howard (2010a), The catalog of halo coronal mass ejections from SOHO, *Sun Geosphere*, *5*(1), 7–16.

Gopalswamy, N., H. Xie, P. Mäkelä, S. Akiyama, S. Yashiro, M. L. Kaiser, R. A. Howard, and J.-L. Bougeret (2010b), Interplanetary shocks lacking type II radio bursts, *Astrophys. J.*, *710*, 1111–1126, doi:10.1088/0004-637X/710/2/1111.

Gopalswamy, N., S. Akiyama, S. Yashiro, and P. Mäkelä (2010c), Coronal mass ejections from sunspot and non-sunspot regions, in *Magnetic Coupling between the Interior and Atmosphere of the Sun, Astrophysics and Space Science Proceedings*, Part 2, 1st ed., edited by S. S. Hasan and R. J. Rutten, pp. 289–307, Springer, Berlin, doi:10.1007/978-3-642-02859-5_24.

Gopalswamy, N., S. Yashiro, H. Xie, S. Akiyama, and P. Mäkelä (2010d), Large geomagnetic storms associated with limb halo coronal mass ejections, in *Advances in Geosciences*, vol. 21, *Solar Terrestrial (ST)*, edited by M. Duldig, p.71, World Science, Singapore.

Howard, R. A., D. J. Michels, N. R. Sheeley Jr., and M. J. Koomen (1982), The observation of a coronal transient directed at Earth, *Astrophys. J.*, *263*, L101–L104, doi:10.1086/183932.

Ipavich, F. M., et al. (1998), Solar wind measurements with SOHO: The CELIAS/MTOF proton monitor, *J. Geophys. Res.*, *103*(A8), 17,205–17,213, doi:10.1029/97JA02770.

Iyemori, T., T. Araki, T. Kamei, and M. Takeda (1992), *Mid-latitude geomagnetic indices ASY and SYM (Provisional) No. 1, 1989*, Data Anal. Cent. for Geomagn. and Space Magn., Kyoto Univ., Kyoto, Japan.

Lario, D., R. B. Decker, E. C. Roelof, D. B. Reisenfeld, and T. R. Sanderson (2004), Low-energy particle response to CMEs during the Ulysses solar maximum northern polar passage, *J. Geophys. Res.*, *109*, A01107, doi:10.1029/2003JA010071.

Lario, D., R. B. Decker, O. E. Malandraki, and L. J. Lanzerotti (2008), Influence of large-scale interplanetary structures on energetic particle propagation: September 2004 event at Ulysses and ACE, *J. Geophys. Res.*, *113*, A03105, doi:10.1029/2007JA012721.

Leblanc, Y., G. A. Dulk, and J.-L. Bougeret (1998), Tracing the electron density from the corona to 1 AU, *Solar Phys.*, *183*, 165–180, 1998.

Lepping, R. P., et al. (1995), The Wind Magnetic Field Investigation, *Space Sci. Rev.*, *71*, 207, doi:10.1007/BF00751330.

Mayaud, P. N. (1968), *Indices Kn, Ks, Km, 1964–1967*, 256 pp., Centre National de la Recherche Scientifique, Paris.

McComas, D. J., et al. (1998), Solar wind electron proton alpha monitor (SWEPAM) for the Advanced Composition Explorer, *Space Sci. Rev.*, *86*, 563–612, doi:10.1023/A:1005040232597.

Menvielle, M., and A. Berthelier (1991), The K-derived planetary indices: Description and availability, *Rev. Geophys.*, *29*, 415–432, doi:10.1029/91RG00994.

Menvielle, M., T. Iyemori, A. Marchaudon, and M. Nosé (2011), Geomagnetic indices, in *Geomagnetic Observations and Models*, *IAGA Special Sopron*

Book Ser. 5, edited by M. Mandea and M. Korte, chap. 8, pp. 183–228, Springer, Dordrecht, Netherlands, doi:10.1007/978-90-481-9858-0_8.

Nitta, N. V., E. W. Cliver, and A. J. Tylka (2003), Low coronal signatures of large solar energetic particle events, *Astrophys. J.*, *586*, L103–L106, doi:10.1086/374613.

Ogilvie, K. W., et al. (1995), SWE, a comprehensive plasma instrument for the Wind spacecraft, *Space Sci. Rev.*, *71*, 55–77, doi:10.1007/BF00751326.

Reames, D. V., C. K. Ng, and A. J. Tylka (2001), Heavy ion abundances and spectra and the larger gradual solar energetic particle event of 2000 July 14, *Astrophys. J.*, *548*, L233–L236, doi:10.1086/319100.

Rodriguez, L., et al. (2009), Three frontside full halo coronal mass ejections with a nontypical geomagnetic response, *Space Weather*, *7*, S06003, doi:10.1029/2008SW000453.

Sauer, H. H. (1993), GOES observations of energetic protons E > 685 MeV: Description and data comparison, *Conf. Proc. 23rd, Int. Cosmic Ray Conf.*, *3*, 250–253.

Schwenn, R. (2006), Solar wind sources and their variations over the solar cycle, *Space Sci. Rev.*, *124*(1–4), 51–76, doi:10.1007/s11214-006-9099-5.

Smith, C. W., et al. (1998), The ACE magnetic field experiment, *Space Sci. Rev.*, *86*, 613–632, doi:10.1023/A:1005092216668.

Sugiura, M. (1964), Hourly values of equatorial *Dst* for the IGY, in *Annals of the International Geophysical Year*, vol. 35, edited by L. V. Berkner et al., pp. 9–45, Pergamon, Oxford, U. K.

Sugiura, M., and T. Kamei (1991), Equatorial *Dst* index 1957–1986, *IAGA Bull.*, *40*, 1–246.

Tylka, A. J., P. R. Boberg, R. E. McGuire, C. K. Ng, and D. V. Reames (2000), Temporal evolution in the spectra of gradual solar energetic particle events, in *AIP Conference Proceedings 528, Acceleration and Transport of Energetic Particles Observed in the Heliosphere*, edited by R. A. Mewaldt et al., p. 147, AIP, New York.

van Nes, P., E. C. Roelof, R. Reinhard, T. R. Sanderson, and K.-P. Wenzel (1985), A major shock-associated energetic storm particle event wherein the shock plays a minor role, *J. Geophys. Res.*, *90*(A5), 3981–3994, doi:10.1029/JA090iA05p03981.

Wang, Y. M., P. Z. Ye, S. Wang, G. P. Zhou, and J. X. Wang (2002), A statistical study on the geoeffectiveness of Earth-directed coronal mass ejections from March 1997 to December 2000, *J. Geophys. Res.*, *107*(A11), 1340, doi:10.1029/2002JA009244.

Wang, Y. M., P. Z. Ye, and S. Wang (2003), Multiple magnetic clouds: Several examples during March–April 2001, *J. Geophys. Res.*, *108*(A10), 1370, doi:10.1029/2003JA009850.

Yashiro, S., et al. (2004), A catalog of white light coronal mass ejections observed by the SOHO spacecraft, *J. Geophys. Res.*, *109*, A07105, doi:10.1029/2003JA010282.

Zhang, J., M. W. Liemohn, J. U. Kozyra, M. F. Thomsen, H. A. Elliott, and J. M. Weygand (2006), A statistical comparison of solar wind sources of moderate and intense geomagnetic storms at solar minimum and maximum, *J. Geophys. Res.*, *111*, A01104, doi:10.1029/2005JA011065.

Zhang, J., et al. (2007), Solar and interplanetary sources of major geomagnetic storms ($Dst \leq -100$ nT) during 1996–2005, *J. Geophys. Res.*, *112*, A10102, doi:10.1029/2007JA012321.

Zhao, X. P., and D. F. Webb (2003), Source regions and storm effectiveness of frontside full halo coronal mass ejections, *J. Geophys. Res.*, *108*(A6), 1234, doi:10.1029/2002JA009606.

Zurbuchen, T. H., and I. G. Richardson (2006), In-situ solar wind and magnetic field signatures of interplanetary coronal mass ejections, *Space Sci. Rev.*, *123*, 31–43, doi:10.1007/s11214-006-9010-4.